Planet. Space Sci., Vol. 36, No. 5, pp. 471–498, 1988
Printed in Great Britain.

0032–0633/88 $3.00+0.00
Pergamon Press plc

THE DEPENDENCE OF HIGH-LATITUDE DAYSIDE IONOSPHERIC FLOWS ON THE NORTH–SOUTH COMPONENT OF THE IMF: A HIGH TIME RESOLUTION CORRELATION ANALYSIS USING EISCAT "POLAR" AND *AMPTE UKS* AND *IRM* DATA

A. ETEMADI and S. W. H. COWLEY
Blackett Laboratory, Imperial College, London SW7 2BZ, U.K.

M. LOCKWOOD, B. J. I. BROMAGE and D. M. WILLIS
Rutherford-Appleton Laboratory, Chilton, Didcot, Oxon OX11 0QX, U.K.

and

H. LÜHR
Institut für Geophysik und Meteorologie, Technischen Universität Carolo-Wilhelmina,
3300 Braunschweig, F.R.G.

(*Received* 9 *November* 1987)

Abstract—In 1984 and 1985 a series of experiments was undertaken in which dayside ionospheric flows were measured by the EISCAT "Polar" experiment, while observations of the solar wind and interplanetary magnetic field (IMF) were made by the *AMPTE UKS* and *IRM* spacecraft upstream from the Earth's bow shock. As a result, 40 h of simultaneous data were acquired, which are analysed in this paper to investigate the relationship between the ionospheric flow and the North–South (B_z) component of the IMF. The ionospheric flow data have 2.5 min resolution, and cover the dayside local time sector from ~09:30 to ~18:30 M.L.T. and the latitude range from 70.8° to 74.3°. Using cross-correlation analysis it is shown that clear relationships do exist between the ionospheric flow and IMF B_z, but that the form of the relations depends strongly on latitude and local time. These dependencies are readily interpreted in terms of a twin-vortex flow pattern in which the magnitude and latitudinal extent of the flows become successively larger as B_z becomes successively more negative. Detailed maps of the flow are derived for a range of B_z values (between ±4 nT) which clearly demonstrate the presence of these effects in the data. The data also suggest that the morning reversal in the East–West component of flow moves to earlier local times as B_z declines in value and becomes negative. The correlation analysis also provides information on the ionospheric response time to changes in IMF B_z, it being found that the response is very rapid indeed. The most rapid response occurs in the noon to mid-afternoon sector, where the westward flows of the dusk cell respond with a delay of 3.9±2.2 min to changes in the North–South field at the subsolar magnetopause. The flows appear to evolve in form over the subsequent ~5 min interval, however, as indicated by the longer response times found for the northward component of flow in this sector (6.7±2.2 min), and in data from earlier and later local times. No evidence is found for a latitudinal gradient in response time; changes in flow take place coherently in time across the entire radar field-of-view.

1. INTRODUCTION

The principal factor governing the structure and dynamics of the Earth's magnetosphere is the large-scale convection driven within it by coupling to the solar wind at the magnetopause (e.g. Cowley, 1980, 1982, and references therein). These flows are communicated along the magnetic field lines to the high-latitude ionosphere, where they are of major importance in terms of ionization transport and Joule heating, as well as in driving thermospheric winds via ion–neutral collisions (Quegan *et al.*, 1982; Rees *et al.*, 1986, and references therein). An important topic of recent study has concerned the degree to which the direction of the interplanetary magnetic field (IMF) influences solar wind–magnetosphere coupling and the consequent convection in the magnetosphere, ionosphere and thermosphere, as postulated theoretically by Dungey (1961). As a result of these studies a dependence of both the form and overall magnitude of the flows on the orientation of the IMF has been clearly established (Heppner, 1972, 1973; Killeen *et al.*, 1985; Baumjohann and Haerendel, 1985; Baumjohann *et al.*, 1986; see also the reviews by Cowley, 1983, 1984, and references therein), thus complementing corresponding results obtained *in situ* at the magnetopause (Rijnbeek et al., 1984; Berchem and Russell, 1984; Cowley, 1986; Paschmann et al., 1986). The ionosphere represents a convenient and relatively accessible place to study these flows and their IMF response, since it mirrors convection occurring over large volumes of the magnetosphere. Ideally, these studies require flow measurements to be made simultaneously over a wide range of latitude and longitude with good (minute or better) time resolution. Practically, however, direct flow data are obtained only from brief low-altitude spacecraft passes, and from a small number of ground-based radar systems. More global, but less direct information can also be obtained from ground-based magnetic measurements which record the perturbations caused by the ionospheric currents driven by these flows.

Electric field or ion drift measurements from low-altitude polar orbiting spacecraft give ~ 10 min "snapshots" of high-latitude ionospheric flows along the spacecraft path, which can be related to concurrent conditions in the solar wind. By combining together the data from many orbits obtained under similar IMF conditions but along different paths, detailed pictures of the flow can be built up, and have been presented on this basis by e.g. Heppner (1977), Heelis and Hanson (1980), Heelis (1984), Burch et al. (1985) and Heppner and Maynard (1987). The results indicate that the primary response of ionospheric flows is to the North–South (B_z) component of the IMF. When the IMF is southward, or at least not strongly northward, the measurements are found to be consistent with a two-cell convection pattern with antisunward flow over the polar cap and return sunward flow at lower latitudes in the auroral zone. The magnitude and latitudinal extent of these flows are observed to increase with progressively more negative values of B_z. In particular, the total cross-polar cap electric potential, which is a measure of the overall ionospheric flow, has been shown to be strongly modulated by IMF B_z (Reiff et al., 1981; Doyle and Burke, 1983; Wygant et al., 1983). In addition, the detailed properties of the flow pattern, such as dawn–dusk flow asymmetries, have been shown to be governed by the East–West component of the (B_y) IMF (e.g. Cowley, 1981, and references therein).

While spacecraft provide rapid snapshots of flows over wide regions of the high-latitude ionosphere, they are unsuited to studies of its temporal response to variations in the IMF and in the magnetosphere. These changes take place on time scales of minutes and tens of minutes compared with spacecraft orbital periods of ~ 1.5 h. Ground-based systems, however, allow continuous monitoring of a given region of the ionosphere, such that the temporal evolution can be studied, albeit in a restricted region. Ground-based and space-based observations are therefore highly complementary in nature and have been successfully combined in some recent studies (Heelis et al., 1983; Lockwood et al., 1986a).

In order to investigate the temporal response of the magnetosphere to changes in the solar wind and IMF, studies of the correlation between the latter parameters and magnetic disturbance indices derived from ground-based magnetometer records (e.g. AE, AL, K_P and D_{ST}) have traditionally been used (Schatten and Wilcox, 1967; Arnoldy, 1971; Tsurutani and Meng, 1972; Burton et al., 1975; Holzer and Slavin, 1979, 1982; Baker et al., 1981, 1983; Clauer et al., 1981; Akasofu et al., 1982; Meloni et al., 1982; Murayama, 1982; Bargatze et al., 1985; Tsurutani et al., 1985). These studies address two basic questions. The first concerns the form of the function of solar wind and IMF parameters which best correlates with geomagnetic activity, which has implications for the nature of the coupling mechanism(s), and the second concerns the time delay of the magnetosphere response. On the first of these topics, it has again been found that functions which emphasize the southward component of the IMF have exhibited the highest correlation coefficients. Among the most consistently highly correlated have been the "half-wave rectifier" functions VB_S and V^2B_S, together with the "epsilon parameter" (Perreault and Akasofu, 1978) given by

$$\varepsilon = VB^2 \sin^4(\theta/2).$$

In these expressions V is the speed of the solar wind, B_S is defined as $B_S = 0$ when IMF B_z is positive and $B_S = B_z$ when B_z is negative, and θ is the polar angle of the IMF vector projected onto the GSM y–z plane, measured from North. A preference for VB_S or V^2B_S has been indicated by some studies (Clauer et al., 1981; Baker et al., 1983; Holzer and Slavin, 1982, 1983; Murayama, 1982; Bargatze et al., 1985). With regard to the time delay, most investigators have found that the magnetic disturbance "output" lags the solar wind/IMF "input" by some 30–60 min, though with an indication of smaller delays of ~ 15 min or less during more disturbed times (Baker et al., 1981, 1983; Clauer et al., 1981; Bargatze et al., 1985). It should be pointed out, however, that all of these studies have used magnetic activity indices which respond principally to the strength of the nightside electrojet currents (i.e. the DP-1 current system). The lengthy delays of ~ 45 min which have been found can then be interpreted as the time scale required for substorm onset in the geomagnetic tail and electrojet intensification following southward turnings of the

IMF. The time scale on which more general magnetospheric and ionospheric circulation is modulated by IMF conditions is much less well established. The magnetic counterpart of the high-latitude twin vortex flows observed in the ionosphere is the DP-2 disturbance system, which is distinguished from DP-1, in particular, by the lack of a strong current concentration in the nightside auroral zone (Nishida, 1968a). It has been well established that DP-2 disturbances are related to the North–South component of the IMF, with Nishida (1968b) finding that high-latitude enhancements occur about 7 ± 1 min after southward IMF turnings impinge upon the Earth's bow shock. Similar short time scales have been found in recent individual case studies by e.g. Pellinen *et al.* (1982), Nishida and Kamide (1983), McPherron and Manka (1985) and Clauer and Kamide (1985). Although the above studies investigated relatively small quantities of data, they are already sufficient to show that more than one time scale is involved in the response of the coupled magnetosphere–ionosphere system to the solar wind, with changes in flow occurring on much shorter time scales (few minutes) than is involved in the substorm process (few tens of minutes). The relative lack of study of the former time scale relative to the latter may presumably be related to the fact that no simple index parameterizing DP-2 has yet been devised, in the same way that e.g. the *AE* index (albeit imperfectly) parameterizes DP-1.

In addition to examining magnetic disturbances measured on the ground, it has become possible more recently to measure ionospheric flows directly using incoherent scatter radars (Doupnik *et al.*, 1972; Evans *et al.*, 1980; Wickwar *et al.*, 1984). Most experiments employed to date have concentrated on deriving profiles of the vector flow over a wide range of invariant latitudes, using multi-point scans with cycle times of typically 15–30 min (Evans *et al.*, 1980; Foster *et al.*, 1981, 1982; Foster, 1983; Oliver *et al.*, 1983; Foster and Doupnik, 1984; Clauer *et al.*, 1984; Jorgensen *et al.*, 1984; Clauer and Banks, 1986; Alcayde *et al.*, 1986; Fontaine *et al.*, 1986). These studies have served to determine the main features of the ionospheric auroral zone flow, but their time resolution has been too low to allow detailed examination of few-minute ionospheric response times.

To overcome these difficulties, the EISCAT "Polar" experiment was devised with the aim of determining vector flows at high latitudes with significantly better temporal resolution than has been generally obtained hitherto (van Eyken *et al.*, 1984; Willis *et al.*, 1986). In this experiment the radar beam is swung successively between two dwell positions directed at low elevation angles to the North of the transmitter site at Tromso, with a full cycle time of 5 min. The data are then analysed to produce a profile of the ionospheric vector flow in the invariant latitude range $\sim 71° - \sim 75°$ (the range over which the radar beams pass through the *F*-region ionosphere), every 2.5 min. The experiment therefore covers a relatively restricted range of latitudes, but has a temporal resolution which is about one order of magnitude better than is typical of previous experiments. In 1984 and 1985 a series of "Polar" runs was conducted in coordination with simultaneous measurements in the solar wind by the *AMPTE UKS* and *IRM* spacecraft. Initial studies on an event-by-event basis have already shown the close correspondences which exist between these data sets, and their potential for studying the form and time scale of ionospheric responses to variations in the direction of the IMF (Rishbeth *et al.*, 1985; Willis *et al.*, 1986; Lockwood *et al.*, 1986b; Todd *et al.*, 1987). The purpose of this paper, therefore, is to present the results of a detailed cross-correlation analysis of the EISCAT "Polar" and the *AMPTE* data. In the next section we will give further details of the "Polar" and *AMPTE* experiments, and the joint data set derived therefrom. By way of introduction to the nature of the observations we will also overview one of the joint experiments which provides further qualitative evidence of the control exerted on high-latitude flows by the North–South component of the IMF. Sections 3–5 then present the quantitative results of our numerical analysis.

2. THE EISCAT "POLAR" AND *AMPTE* DATA SETS

The EISCAT "Polar" experiment was devised with the principal initial aim of measuring flows in the dayside auroral zone and polar cusp ionosphere with good temporal resolution (van Eyken *et al.*, 1984; Willis *et al.*, 1986). Since the cusp is usually located far to the North of the EISCAT transmitter site at Tromso (invariant latitude 66.3°), where the EISCAT tristatic geometry is unfavourable, a beam-swinging experiment is employed. The radar beam is swung successively between two pointing directions which have a low elevation angle (21.5°) and which are directed in azimuth 12° on either side of the local *L*-shell meridian (geographic azimuth 344°). Equal ranges along the two pointing directions are thus located at nearly equal invariant latitudes. The radar antenna dwells for 2 min at each pointing direction, and takes 30 s to complete each swing manoeuvre. The full cycle time of two dwells and two swings is therefore 5 min.

As mentioned above, the range of invariant latitudes covered by the experiment corresponds to the

Table 1

Gate number	Range (km)	Height (km)	Invariant latitude
1	525	211	70.8
2	600	243	71.4
3	675	277	72.0
4	750	311	72.6
5	825	346	73.2
6	900	382	73.8
7	975	418	74.3
8	1050	455	74.9
9	1125	493	75.4

Values given correspond to the centre of each range gate.

range over which the oblique radar beams pass through the *F*-region ionosphere. In order to give latitudinal resolution within this range, the return signal is divided into a number of contiguous gates. The centre of gate 1 is located at a range of 525 km, a height of 211 km and an invariant latitude of 70.8°. The centres of subsequent gates are then displaced successively by distances of 75 km along the beam, corresponding to increments of approximately 35 km in height and 0.6° in invariant latitude. For much of the data used in this study (obtained mainly in the dayside hours where the *F*-region ionosphere is relatively dense), useful signal-to-noise is present out to at least gate 7, located at a range of 975 km, a height of 418 km and an invariant latitude of 74.3°. Under these conditions, therefore, useful measurements are generally obtained over the latitude range ~71°–~74°, with a latitudinal resolution of ~0.6°. The ranges, heights and invariant latitudes of the "Polar" gates are given in Table 1.

Vector flows are determined from the "Polar" data by combining the line-of-sight velocities measured in the two pointing directions for each of the range gates. It is assumed in the analysis that the North–South and East–West components of the flow transverse to the Earth's magnetic field are the same in the two scattering volumes, these being separated (in longitude) by ~200 km for gate 1, increasing to ~380 km for gate 7. It is also assumed that the (unmeasured) field-aligned component of the flow is zero, since these flows are expected to be generally small compared with the flows transverse to the field. The experiment is in any case insensitive to flows along the field because of the large aspect angle between the field and the radar beam (~74°). With these assumptions, the line-of-sight velocities measured in each gate during each dwell period are combined with the average of the values obtained in the same gate in the two adjacent dwells at the other pointing direction. The latter average is taken in order to form an appropriately time-centred value. A latitude profile of the vector flow is thus obtained every 2.5 min.

During autumn 1984 and summer 1985 a series of "Polar" runs was conducted in coordination with *AMPTE UKS* and *IRM* observations of the solar wind and IMF, the spacecraft being located immediately upstream of the Earth's bow shock (Bryant *et al.*, 1985). These experiments resulted in the acquisition of approximately 40 h of simultaneous data, whose distribution is shown in Fig. 1. The lower panel shows the U.T. coverage on each of the five experiment days, which were 29 September, 25 and 27 October 1984, and 27 and 29 August 1985. The open areas bounded by the solid lines correspond to the periods during which the "Polar" experiment was run on each day, the magnetic local time (M.L.T.) of the measurements being given approximately by adding 2.5 h to U.T., as indicated in the M.L.T. scale at the top of the figure. The hatched areas bounded by the dashed lines then indicate the intervals during which IMF data were obtained, specifically by the *UKS* magnetometer (Southwood *et al.*, 1985) during the experiments in 1984, and by the *IRM* magnetometer (Lühr *et al.*, 1985) during the experiments in 1985. This information is combined in the upper panel of Fig. 1, which shows a histogram of the number of experiments from which data are available vs U.T. (M.L.T.), using the same format as the lower panel. It can be seen that the simultaneous data are mainly confined to the dayside hours, from ~07–17 U.T., corresponding to ~09 to ~19 M.L.T. (This limitation results from the fact that data were only acquired from the *AMPTE* spacecraft by ground stations in the European sector, close to the meridian of the EISCAT system.) Since the reversal in the predominant direction of dayside flow from eastward to westward has been found to take place at least 2–3 h prior to local noon in the "Polar" data (see e.g. Willis *et al.*, 1986), most of the data considered here thus relate to the morning flow reversal region, and the westward flows of the "dusk" auroral zone flow cell. The joint data set contains little information about the response of the dawn cell.

Visual inspection of the data immediately reveals the common occurrence of apparently corresponding features. A particularly obvious example has been discussed in detail by Rishbeth *et al.* (1985) and Lockwood *et al.* (1986b), in which a sharp southward turning of the IMF (observed at 11:07 U.T. on 27 October 1984) was followed 12 min later by the appearance of strong westward flows across the "Polar" field-of-view in the mid-afternoon sector. Additional examples have also been presented by Todd *et al.* (1988). Qualitative descriptions of the joint

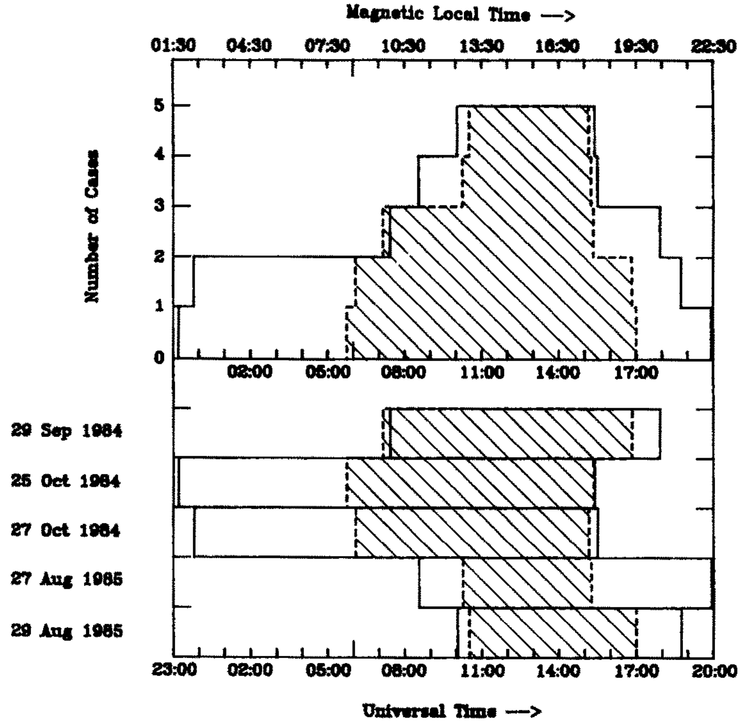

FIG. 1. GRAPH SHOWING THE DISTRIBUTION OF DATA USED IN THIS STUDY.
The lower panel shows the intervals during which EISCAT and *AMPTE* data were obtained on each joint experiment day, where the horizontal axis is U.T.. M.L.T. in the "Polar" field-of-view may be found by adding approximately 2.5 h to these values, as indicated in the M.L.T. scale along the top border of the plot. The open areas bounded by solid lines indicate the intervals of the EISCAT "Polar" experiments (note that the experiments on 25 and 27 October 1984 actually started shortly before the end of the previous day), while the hatched area bounded by the dashed line indicates the availability of *AMPTE* data (*UKS* data for the experiments in 1984 and *IRM* data for those in 1985). This information is combined in the upper plot which shows a histogram of the number of experiments from which data are available (same format as in the lower panel) vs U.T. (M.L.T.) hour.

data for the experiments conducted on 29 September, 25 and 27 October 1984 and 29 August 1985 have previously been published by Willis *et al.* (1986) and Todd *et al.* (1988). Therefore, we will present here a brief overview of observations on 27 August 1985, which have not previously been published. The principal aim of the discussion is to provide a more detailed introduction to the nature of the joint EISCAT "Polar"/*AMPTE* observations. At the same time we shall also offer further qualitative evidence of the correlation between the EISCAT and IMF data sets, thus providing the motivation for the cross-correlation analysis presented below.

Figure 2 shows the data obtained during the joint EISCAT/*AMPTE* experiment on 27 August 1985. In the upper part of the figure we show IMF data obtained by the *IRM* spacecraft [located at GSE $(X, Y, Z) = (10, 15, -3)$ R_E upstream of the shock] between 10:16 and 15:15 U.T. These data are plotted in the form of cartesian components in GSM coordinates, which are routinely available as 5 s averages, but have been further averaged here to 1 min values in this overview plot. It can be seen that the IMF B_z component is predominantly positive during the experiment, though the interval is punctuated by relatively brief (~ 15 min) periods during which near-zero or negative values of B_z occur. Plasma data acquired during the interval (kindly provided by Dr G. Paschmann) indicate a very steady solar wind flow with a bulk speed of ~ 650 km s^{-1} and a proton number density of ~ 2 cm^{-3}. In the lower part of the figure we show the 2.5 min resolution ionospheric flow vectors which were derived from the "Polar" data using the method described above. In order to reduce congestion in this plot the predominantly East–West directed flow vectors have all been rotated clockwise through 90°, such that a westward flow vector points upward, a northward flow vector to the right (as indi-

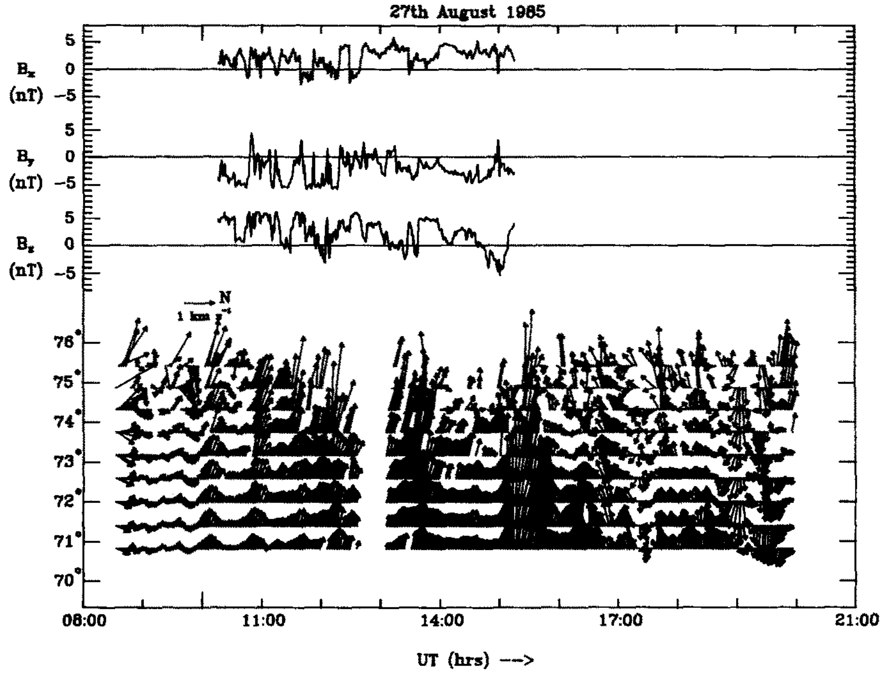

FIG. 2. OVERVIEW PLOT OF THE IMF AND IONOSPHERIC FLOW DATA OBTAINED DURING THE JOINT EISCAT/*AMPTE* EXPERIMENT ON 27 AUGUST 1985.

The upper part of the figure shows 1 min averages of the IMF data obtained by the *AMPTE IRM* spacecraft upstream of the Earth's bow shock (radial distance 18.7 R_E, GSE latitude $-8°$, GSE local time 15.8 h). The data are shown as GSM components. The lower part of the figure shows 2.5 min resolution ionospheric flow vectors obtained simultaneously by the EISCAT "Polar" experiment. The flow vectors have been rotated clockwise through 90° to help avoid clutter. Magnetic local time may be found approximately by adding 2.5 h to U.T.

cated by the arrow), while an eastward flow vector points downward. The vectors thus actually point in the direction of the ionospheric electric field associated with the flow. A vector is plotted for a given dwell and given gate provided the signal-to-background ratio exceeds 0.8%.

Flow measurements were obtained from 08:33 to 19:55 U.T. ($\sim$ 11:00 to 22:30 M.L.T.), and encompass four principal regions. With increasing local time these are the dayside region equatorward of the auroral zone flow cells (08:33 to $\sim$10:00 U.T.), the dusk cell of predominantly westward flow ($\sim$10:00 to $\sim$15:30 U.T.), the evening boundary region between the dusk cell and the polar cap ($\sim$15:30 to $\sim$19:00 U.T.), and a region of eastward flow in the nightside auroral zone ($\sim$19:00–19:55 U.T.). At the start of the experiment ($\sim$ 11:00 M.L.T.) the "Polar" field-of-view is located in the first of these regions where a flow-burst event is in progress, characterized by a short-lived burst of rapid (e.g. $\sim$500 m s^{-1} in gate 4) poleward-directed flow (Todd *et al.*, 1986, 1988). After the burst has died away, the flows remain very small for more than an hour, until a burst of westward flow appears, starting shortly before 10:00 U.T. ($\sim$12:30 M.L.T.). Westward flows are then observed essentially continuously across the field-of-view until $\sim$15:30 U.T., when the weak flows of the polar cap boundary region start to appear in the poleward gates. The region of westward flow corresponds to the dusk auroral zone flow cell, in which it can be seen that the flow vectors, though of consistent orientation, are of very variable magnitude. Comparison with the simultaneous IMF data then shows an almost one-to-one correspondence between peaks in the flow speed and intervals of near-zero and negative B_z, with the peaks in flow appearing roughly 10 min after reductions in the value of B_z. For example, the reduction in B_z from $\sim$5 to $\sim$1 nT which occurs between 10:30 and 10:45 U.T. is followed by a burst of westward flow (peaking e.g. at $\sim$700 m s^{-1} in gate 4) between 10:40 and 11:05 U.T. Similar flow enhancements also follow the B_z reductions centred approximately on 11:25, 12:00, 13:15 and 14:55 U.T. Some local time differences in the ionospheric response to the IMF may, however, be noted for future reference. In the noon and early afternoon sector [up to ~11:00 U.T. (~13:30 M.L.T.) in Fig. 2] the flow falls very nearly to zero when IMF B_z becomes large and positive (above, say 1 or 2 nT), whereas later in the afternoon weak westward flows remain even under these conditions (e.g. between 13:45 and 14:45 U.T. in Fig. 2). These observations indicate that weak quiet-time flows persist during intervals of strongly positive IMF B_z, but that the "Polar" field-of-view lies equatorward of them until after ~13:30 M.L.T. (Observations on other days indicate that, correspondingly, the eastward flows of the quiet-time dawn cell recede beyond the farther gates after ~10:00 M.L.T. in the morning sector.)

When the "Polar" field-of-view lies within the central and equatorward portions of the flow cells a relatively simple positive correlation is observed between the flow speed and IMF B_z, as discussed above. However, Fig. 2 shows that at later local times the field-of-view moves into the poleward region of the cell where flow speeds decrease with increasing latitude. In this region more complex flow responses may be anticipated, because although enhanced coupling at the magnetopause will increase overall flow magnitudes, it will also in general result in an expansion of the size of the flow system, due in part to the production of new open flux. This effect will then cause the flow to *weaken* with increasingly negative IMF B_z in the region near the polar cap boundary, since there the flow speeds decrease rapidly and reverse in sense with increasing latitude. A simple model which illustrates this expected behaviour, and which will be compared with the results presented in Section 3, is shown in Fig. 3. At the top of the figure we show an assumed variation of the auroral zone flow with latitude for several values of IMF B_z. At each B_z the variation of the flow speed with latitude is for simplicity modelled by a section of a sinusoid, which increases from zero at low latitudes to a peak at the centre of the auroral zone and then declines and turns negative. The region of reversed flow corresponds to the polar cap. The profile on the right side of the diagram, marked "$\geqslant 0$", is that assumed for positive B_z, taken for simplicity to be independent of the field magnitude. As B_z becomes increasingly negative we assume that the overall flow speeds are enhanced, that the width of the auroral zone becomes larger, and that its high-latitude boundary (where the flow speed crosses zero) is displaced equatorward as a result of an expansion of the polar cap. These model assumptions are supported qualitatively by the results cited previously in the Introduction. The leftmost of the profiles (shown by the solid line marked "-4") is taken to be that corresponding to the largest commonly occurring negative B_z value, such that this flow profile represents the most developed pattern commonly encountered. In the data set employed here B_z is generally confined to the range ± 4 nT (cf. Fig. 4), thus explaining the choice of labelling employed in Fig. 3.

Given this simple model, the graphs plotted beneath the flow profiles then show how the flow will respond to IMF B_z at the various latitudes indicated by the lettered arrows. These graphs are labelled V_E (for eastward flow) and are shown as negative values (for the westward flows of the dusk cell) in order to correspond to the format of the data to be presented in the next section. Latitudes (a) and (b) correspond to points located at and equatorward of the peak in the most expanded cell ($B_z = -4$ nT), and show a simple monotonic increase in flow speed as B_z becomes increasingly negative (over the range of B_z values considered). The main difference between positions (a) and (b) is that (b) also lies within the region of flows for the most contracted ($B_z > 0$) cell, such that the flow speed remains non-zero as B_z becomes positive. Similar behaviour is also found poleward of the peak in the "most expanded" cell, but the flow response to B_z becomes increasingly weak with increasing latitude, as shown in graph (c). Indeed, as the "cross-over" point is approached the behaviour becomes non-monotonic, and the flow speed starts to decline with decreasing B_z, after an initial increase. The "cross-over" point is the point where the flow speed for the "most expanded" and the "most contracted" cell are equal at a given latitude (see upper diagram of Fig. 4). Equatorward of this point there is an overall increase in speed in making the transition from the "most contracted" to the "most expanded" cell, while at the "cross-over" point itself there is no net change, and the flow speed varies only very weakly with B_z as shown in graph (d). Poleward of the "cross-over" point there is an overall decrease in flow speed as B_z decreases from zero to -4 nT, such that the flow speed becomes anticorrelated with negative B_z as shown in graph (e). We note, however, that the flow speed response to B_z is smaller here than in the equatorward region [cf. graphs (a) and (b)] because of the overall increase in flow speed assumed. This effect adds to the increase in flow due to auroral zone expansion in the equatorward region, but subtracts from the reductions in flow resulting from the cell expansion in the poleward region. As a result of this effect we do not therefore expect the anticorrelations occurring in the poleward part of the cell to be as marked as the positive correlations in the equatorward region. We also note that while the "cross-over" point in our simple model has been taken to be colocated with

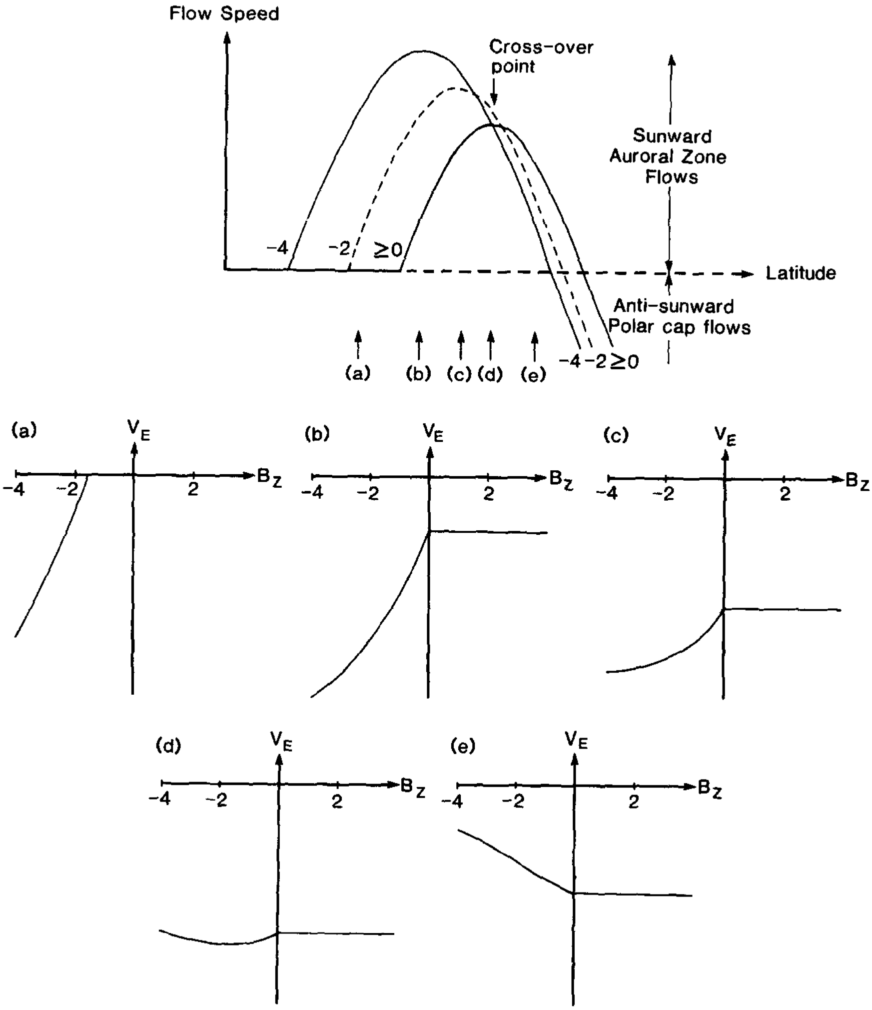

Fig. 3. Sketch showing a simple model of the flow profile vs latitude in the auroral zone flow cells and its variation with IMF B_z (upper diagram), and the consequent variation of the flow speed with B_z at the various arrowed and lettered latitudes (lower graphs).
As B_z becomes increasingly negative the flow profile is taken to increase in overall magnitude, expand in size, and shift towards the equator. The last effect results in a reversal in the sense of the flow speed variation with IMF B_z between the regions equatorward and poleward of the cross-over point [at latitude (d)].

the peak in the "most contracted" cell (see upper diagram), it could also occur somewhat poleward or equatorward of this point, depending on the detailed behaviour of the flow profiles as B_z changes.

In summary, it can be seen from this simple model that when the radar field-of-view is located equatorward of the peak in the "most expanded" cell a strong positive correlation between flow speed and negative IMF B_z is anticipated, arising from the combined effects of the expansion in the flow pattern and the enhancement in the flow speeds. A positive correlation should continue to be present poleward of the peak in this cell, though rapidly diminishing in magnitude as the "cross-over" point is approached in the vicinity of the peak in the "most contracted" cell. At this point the effects of cell expansion and flow enhancement just cancel. Poleward of this point the flow speed should increasingly anticorrelate with B_z as the boundary of the polar cap is approached, due to the dominant effect of the expansion of the flow pattern. However, these decreases should be partly offset by the increase in flow speed which occurs, so that the anticorrelation effect should be weaker than the positive correlations which are present in the equatorward region.

These considerations will be borne in mind when discussing the results presented in the next section. We should point out here, however, that due to the restricted latitudinal coverage of the "Polar" field-of-view, only some of the above range of behaviour will be observable in any particular local time sector. However, owing to the nightside offset between the centre of the polar cap and the magnetic pole, the radar field-of-view will scan through these various regions with increasing local time, e.g. being generally located in the equatorward region of the flow cells in the noon and early afternoon sector and in their poleward region nearer to dusk (cf. Fig. 2). As the radar rotates from the noon to the dusk meridian, therefore, the form of the correlation between the flow speed and IMF B_z in each range gate should vary systematically from strong positive correlations near to noon, to weaker anticorrelations nearer to dusk, with a region where there is little IMF B_z dependence of the flow between. This pattern should be observed in each gate, but at successively earlier local times at successively higher latitudes.

Returning now briefly to Fig. 2, it can be seen from the latitudinal gradients in the flow that (at least for the lower gates where the behaviour is clearest) the radar is located within the equatorward and central portions of the dusk cell (where the flows increase or remain relatively constant with latitude) until ~15:30 U.T., and in the poleward portions where the flows decrease with latitude thereafter (until ~19:00 U.T.). A positive correlation between the flow speed and IMF B_z is indeed apparent in the former region, as discussed above, but it is impossible to relate the flow modulations observed in the latter region to concurrent IMF B_z variations (where anticorrelation is expected) due to the lack of *AMPTE IRM* coverage beyond 15:15 U.T. It may be noted, however, that an example of apparent anticorrelation between ionospheric flow speed and negative IMF B_z has previously been presented by Todd *et al.* (1988) from data acquired in the dusk polar cap boundary region on 29 August 1985 (see their Fig. 6e).

In summary, the results presented in Fig. 2 (together with those discussed previously by Rishbeth *et al.*, 1985; Lockwood *et al.*, 1986b and Todd *et al.*, 1988) show that the pattern of dayside flows at "Polar" latitudes responds clearly and promptly to the North–South component of the IMF. We note, however, that the flow response is expected to depend upon latitude and local time, and should not always take the form of a simple positive correlation. An important additional feature of the data which should also be noted from Fig. 2, is that the changes in flow resulting from changes in B_z appear to occur simultaneously across the "Polar" field-of-view, with no noticeable delays in the lower latitude gates compared with those at higher latitudes (within the 2.5 min resolution of the data). This suggests that, following a change in IMF B_z, the new flow pattern develops as a whole, coherently in time, rather than by an intensification and equatorward expansion of the pre-existing flow system. As mentioned above, the delay in the ionospheric response to changes in IMF B_z measured by the *AMPTE IRM* spacecraft is about 10 min in Fig. 2, but more than half of this delay can already be accounted for simply in terms of the IMF propagation time between the spacecraft and the subsolar magnetopause, as will be discussed further in Section 3 below. The principal purpose of this paper, then, is to follow up these findings with a quantitative cross-correlation analysis which is able to examine the statistical significance of the relations noted visually, and which is also able to assess more accurately the time lags involved. In the next three sections, therefore, we shall present the principal results of our cross-correlation analysis of the EISCAT and *AMPTE* data sets.

3. CROSS-CORRELATION ANALYSIS

In this study the data from all the joint EISCAT/*AMPTE* experiments have been combined together before being divided into different U.T. (M.L.T.) intervals for analysis. In combining the data from different experiment days, adjustment must first be made for the time taken by the IMF signal to propagate from the spacecraft to the magnetosphere, since this varies from experiment to experiment. We have therefore carefully estimated the time taken by the field changes to propagate from the spacecraft to the subsolar magnetopause and have shifted the time axes of the IMF data by this amount. The cross-correlation values at zero time lag shown in the figures in this section thus correspond to those derived by combining the ionospheric flow data directly with the shifted IMF values, these representing (to the best of our ability to estimate) a measure of the instantaneous field at the subsolar magnetopause (modified, of course, by flow compression effects). Any delays of the ionospheric response to the IMF input relative to zero lag will then correspond only to the time taken by the coupling processes to act to the magnetopause, and then for their effects to propagate to the "Polar" field-of-view.

To estimate the time shift of the IMF data, use is

TABLE 2

Experiment date	Spacecraft position GSE (X, Y, Z) Earth radii			Solar wind speed (km s^{-1})	Solar wind density (cm^{-3})	IMF time shift (min)
29 Sept. 1984	18.3	−0.4	0.4	400	5	8.8
25 Oct. 1984*	17.2	−7.2	0.0	600	3	4.9
27 Oct. 1984*	17.3	−6.5	−0.2	450	5	6.8
27 Aug. 1985	10.3	15.4	−2.7	650	2	5.5
29 Aug. 1985	10.5	14.9	−2.6	650	3	5.3

* Experiment started on previous day.

made of the known position of the spacecraft and the values of the solar wind bulk speed and density measured *in situ* by the *IRM* fast plasma analyser. The latter measurements are used to estimate the subsolar positions of the bow shock and magnetopause from the empirical models of Fairfield (1971), Formisano *et al.* (1979) and Formisano (1979), from which the IMF propagation times in the solar wind and in the magnetosheath can be calculated. One uncertainty in the calculation arises from the unknown orientation of the planes in which the IMF is constant. We have therefore made two estimates of the time shift, assuming first that these planes are orthogonal to the Earth–Sun line, and second that they lie at the garden-hose angle, and have then taken the average. The uncertainty in the shift arising from this cause is estimated to be about ± 1 min. During these experiments the *AMPTE UKS* and *IRM* spacecraft monitoring the IMF were close to apogee (just upstream from the bow shock) and hence slowly moving, while the bulk speed and density of the solar wind were also nearly constant over the intervals of observation. Consequently, in view of the uncertainty in the estimate, a constant value of the time shift has been employed for each of the experiment days used in this study. The derived values are given in Table 2, together with the data from which they were obtained. It can be seen that the estimated shifts are typically about 6 min (as indicated in the discussion of Fig. 2 in Section 2). The major component of the shift comes from the time taken by the flow to cross the subsolar magnetosheath, at a speed of, on average, one eighth of the upstream solar wind value. [Gas-dynamic models of the solar wind interaction with the magnetosphere (Spreiter and Stahara, 1980) show that the flow speed drops by a factor of four at the subsolar shock, and subsequently decreases approximately linearly with distance in the magnetosheath between the shock and the subsolar magnetopause.]

In the main analysis to be reported here, and illustrated in Fig. 4, the "Polar" data were divided into successive 2 h intervals and cross-correlated with the IMF data using relative lags between the two data sets in the range ± 2.5 h. Here positive lags imply "Polar" velocities lead the IMF (which is, of course, unphysical), while negative lags imply that the IMF leads the ionosphere. Cross-correlation coefficients were computed for each gate separately with 30 s resolution in the lag time, appropriately centred IMF parameters being calculated from the 5 s data for this purpose. The IMF parameter we have used in this analysis is V^2B_S (where, somewhat unconventionally, we have treated B_S as a negative quantity), since, as shown in the Appendix, of the functions usually considered, this parameter generally gives the highest peak cross-correlation coefficients.

In Fig. 4a we show results for the 2 h interval centred on 10:00 M.L.T., the earliest period for which data are available. On the left-hand side of the figure we show correlograms, derived as described above, in which values of the correlation coefficient are plotted vs time lag between the ionospheric and IMF data sets (the latter shifted to the arrival time at the magnetopause as described above) for gates 1, 3 and 5. The solid and dashed lines show the correlation coefficients for the East–West and North–South components of flow (taken as positive towards the East and towards the North) and V^2B_S, respectively, while the dot-dashed lines indicate the 99.9% statistical significance level derived from Student's t-test method. On the right of the figure we show the related scatter plots of the eastward component of flow V_E (crosses) and the northward component V_N (squares) vs $(V/500)^2B_z$, where the speed of the solar wind (V, in km s^{-1}) has been introduced into the latter quantity in order to correspond to the function V^2B_S used in the correlation analysis. (It should be noted, however, that the inclusion of V^2 in this context does not have a strong effect on the results presented. Consequently, in the text below we shall for simplicity often refer to the dependence of flow behaviour "on IMF B_z", even though the quantities actually employed throughout are V^2B_S in the correlograms and V^2B_z in the scatter plots and quantities derived therefrom.) The scatter plots have been produced using the lag time between the data sets indicated by the position of the peak correlation coefficient in the correlograms (for V_N and V_E separately), the values used being given in the figure. Where no single obvious peak occurs above the 99.9% significance level, the scatter plot has been drawn using a nominal lag of 5 min for V_E and 10 min for V_N, these representing "round numbers" which are typical of the data set as a whole. Use of a nominal value is indicated by placing a star against the lag given in the scatter plot. The solid and dashed lines in the scatter plots then show the result of fitting a parabola through the V_E and V_N data, respectively (thus corresponding to the solid and dashed lines in the correlogram), using a quadratic least-squares fit. Finally, the fitted lines are combined together in one plot at the bottom of the figure, so that the behaviour in different range gates (latitudes) may be readily compared.

With this introduction to the format of Fig. 4a we now turn to its contents, and begin by noting that the local time sector under consideration (09:00–11:00 M.L.T.) often corresponds in the "Polar" data to the region between the main auroral zone flow cells where the East–West component of flow reverses in sign (Willis *et al.*, 1986). We note at the outset, therefore, that the remarks made in the previous section relating to Fig. 3, which were concerned principally with the main part of the auroral zone flow cells, are not wholly germane here. Considering the correlograms for V_E (shown by the solid lines), it can be seen that although a broad region of positive correlation generally exists for negative lag (IMF leads the ionosphere), the correlograms for all three gates have a ragged appearance, with multiple peaks which barely reach the 99.9% significance level. The V_E scatter plots (plotted with the nominal 5 min lag) then correspondingly show only relatively weak dependences on IMF B_z, superimposed upon considerable scatter. Nevertheless, the mean flows indicated by the solid lines do show that V_E decreases by small amounts with decreasing IMF B_z in all three gates. When IMF B_z is positive, flows are weak and westward (V_E negative) in the lower gates, but reverse in sign to become eastward (V_E positive) in gate 5, indicating the presence of the dawn auroral zone flow cell at the higher latitudes in this morning M.L.T. sector. However, when IMF B_z is negative, V_E declines to become negative (westward on average) in all three gates, with strongest flows being found at lowest latitudes, as can be seen in the combined plot at the foot of the figure. The reversal in sign of V_E in gate 5 as B_z changes from positive to negative suggests that the morning East–West flow reversal shifts westward to earlier local times across ~10:00 M.L.T. as B_z changes from positive to negative, as will be discussed further in Section 4. Overall, however, these flows show only a modest response to IMF B_z, and of themselves would not convincingly demonstrate strong IMF control.

On the other hand, the correlograms for V_N contain a sharp peak in all three gates, with a lag indicating an ionospheric response delay (relative to the arrival of southward fields at the magnetopause) of about 12 min. Note that there appears to be little systematic variation of the response delay with latitude, in agreement with the conclusions reached in Section 2 based upon visual inspection of the data. The related scatter plots show that V_N increases from values which are essentially zero (or weakly positive in the upper gates) when B_z is positive, to a few hundred metres per second (again positive) when B_z is a few nanoteslas negative, with the northward flows increasing somewhat in speed with increasing latitude, as again indicated by the plot at the bottom of the figure. Thus in the local time sector which lies in the vicinity of the morning East–West flow reversal we find a strong dependence of the North–South component of the flow on IMF B_z, but only rather weak dependence, and much scatter, in the East–West component.

Results for the following 2 h interval centred on 12:00 M.L.T. are shown in Fig. 4b, in the same format as Fig. 4a. Qualitative examination of the data in this interval (e.g. that presented by Willis *et al.*, 1986) indicates the appearance of relatively weak Northwestward-directed flows in response to southward turns of the IMF, with little flow present for strong northward fields, as previously noted above in the discussion of Fig. 2. Correspondingly, the correlograms for all three gates show that a prominent peak (well above the 99.9% significance level) now occurs for both V_N and V_E, with an ionospheric response delay of about 5 min for each. This delay is rather shorter than found in the previous M.L.T. sector, but is again seen to be nearly independent of latitude. The scatter plots appropriate to these peaks plotted on the right of the figure show that, as expected, flow speeds are small when IMF B_z is strongly positive, only weak westward flows of ~100 m s^{-1} then being present whose magnitude is not strongly dependent on latitude or B_z. Clearly the radar field-of-view lies equatorward of the main quiet-time flow pattern under these conditions. However, flow speeds monotonically increase in magnitude as IMF B_z becomes increasingly negative. Since the magnitude of V_E is generally much larger than V_N in each gate, the flow is predominantly westward-directed, though with a small northward tilt, and obviously corresponds to the "dusk" auroral zone flow cell. It is also clear from the plot at the bottom of the figure that both components of the flow now increase in magnitude with increasing latitude over the radar field-of-view, suggesting a location within the equatorward portion of the dusk flow cell excited by coupling at the magnetopause, even for the most negative values of IMF B_z occurring in this sector (~ -5 nT). These results thus clearly correspond to graph (a) in Fig. 3, though the onset of flow near the equatorward edge of the cell appears to be rather more gradual than in our simple model.

The correlograms for the 2-h period centred on 14:00 M.L.T. are shown in Fig. 4c, and exhibit peaks for both V_N and V_E which are even more obvious than in the previous interval. The peaks in V_E occur with an ionospheric response delay of ~ 5 min, with those for V_N occurring a few minutes later, at least for the lower two gates. It will be shown in Section 5 below that the delay in V_N is, in fact, generally longer than that in V_E in the afternoon sector. This result implies that although flow is excited very rapidly in the day-side ionosphere following southward turnings of the IMF, the form of the flow does evolve over the subsequent ~ 5 min interval, in particular turning from westward to north-westward in the mid-afternoon sector. This behaviour was previously noted by Willis *et al.* (1986), Lockwood *et al.* (1986b) and Todd *et al.* (1988) for the much-studied 11:19 U.T. ($\sim$ 13:50 M.L.T.) flow onset on 27 October 1984, the data for which do, of course, form part of that shown in the present figure. The other main point to note about the figure is that, unlike the previous two intervals where the flow drops essentially to zero when IMF B_z becomes significantly positive, the westward flow component in this sector remains finite (and, indeed, relatively constant) in these circumstances. It may be recalled from the discussion of Fig. 2 in the previous section that weak flows continue to be present in that data when IMF B_z is positive for local times later than $\sim$13:30 M.L.T., in agreement with the more general results obtained here. Large enhancements in the flow speed appear when IMF B_z is negative, however, reaching values (for a given B_z) considerably in excess of those found in the previous M.L.T. sector. This result indicates that the radar field-of-view lies more centrally within the flow cell in this local sector than previously, in the region just equatorward of the peak flow of the "most expanded" cell. The latter conclusion is indicated by the weak (compared with Fig. 4b) poleward-directed gradient in flow speed observed for negative B_z, as will be further substantiated in the next section. These results clearly relate to graph (b) in Fig. 3. The main conclusion to be drawn, however (as well as from Figs 4a and 4b), is that they provide strong quantitative support for the view reached earlier from visual inspection of the data that the dayside flows are closely controlled by the North–South component of the IMF, and that they respond to changes in this component within a few minutes (~ 5 min) of their appearance at the magnetopause.

Figure 4d shows results for the following 2 h period centred on 16:00 M.L.T., which clearly shows quite different behaviour from the two previous M.L.T. sectors. The results for gate 1 are essentially similar to those in the previous figure, and show a flat response for positive B_z, and a rapid, and on average monotonic rise as B_z becomes negative. In fact, the response is very nearly the same as in gate 5 in Fig. 4c, indicating a location close to the peak in the "most expanded" cell [graph (b) in Fig. 3] in this local time sector. The response delay is about 6 min for V_E and 20 min for V_N. The data for gate 3 also show a positive correlation between the flow speed and negative B_z, though it is weaker than in gate 1, and there is no response in V_N. It should be noted that when IMF B_z is positive the flow speed in this gate is higher than in

FIG. 4a. THIS FIGURE SHOWS THE RESULTS OF THE CROSS-CORRELATION ANALYSIS BETWEEN THE NORTH–SOUTH (V_N) AND EAST–WEST (V_E) COMPONENTS OF IONOSPHERIC FLOW AND V^2B_S, FOR THE 2 h INTERVAL OF MAGNETIC LOCAL TIME FROM 09:00 TO 11:00 M.L.T. (06:30–08:30 U.T.).

On the left of the figure we show the correlograms for gates 1, 3 and 5 for lags of ± 2.5 h between the ionospheric and solar wind data sets, with a lag resolution of 30 s. The solid line is the correlogram for V_E, and the dashed line the correlogram for V_N. Negative lag means that the solar wind leads the ionosphere, and vice versa for positive lag (unphysical). The dot-dashed lines in these plots indicate the 99.9% significance level. On the right of the figure we show scatter plots of the two velocity components V_N (squares) and V_E (crosses) vs $(V/500)^2B_z$, where V is the solar wind speed in km s^{-1}. These have been plotted using the lag time indicated by the peak in the correlogram, separately for V_N and V_E (the upper and lower numbers, respectively, in the scatter plots). Where no obvious peak occurs above the 99.9% confidence level the plots are produced for a nominal lag of 300 s for V_E and 600 s for V_N (indicated by the starred values given in the plots), values which are typical of the data set as a whole. The solid lines fitted to the data are parabolae obtained from a quadratic least-squares fit. Solid lines again refer to V_E and dashed lines to V_N. These fitted lines are plotted together in the diagram at the foot of the figure, according to the key given, so that latitudinal variations in the mean flows as a function of B_z can be readily assessed.

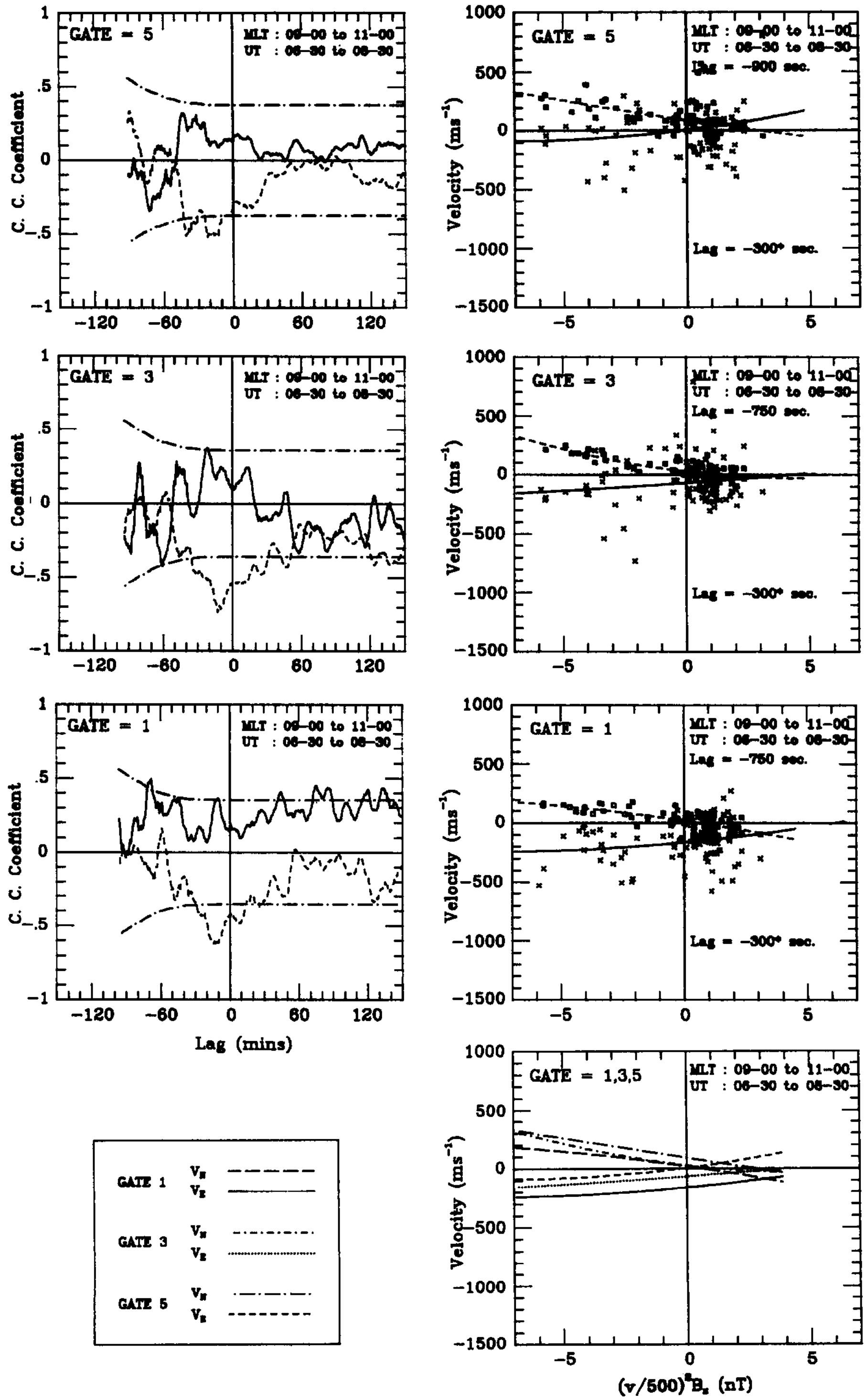
GATE = 5
MLT : 09-00 to 11-00
UT : 08-30 to 09-30
C. C. Coefficient
Lag = -900 sec.
Lag = -300* sec.
Velocity (ms^{-1})
GATE = 3
Lag = -750 sec.
GATE = 1
Lag (mins)
GATE = 1,3,5
GATE 1
GATE 3
GATE 5
V_N
V_E
$(v/500)^2 B_z$ (nT)

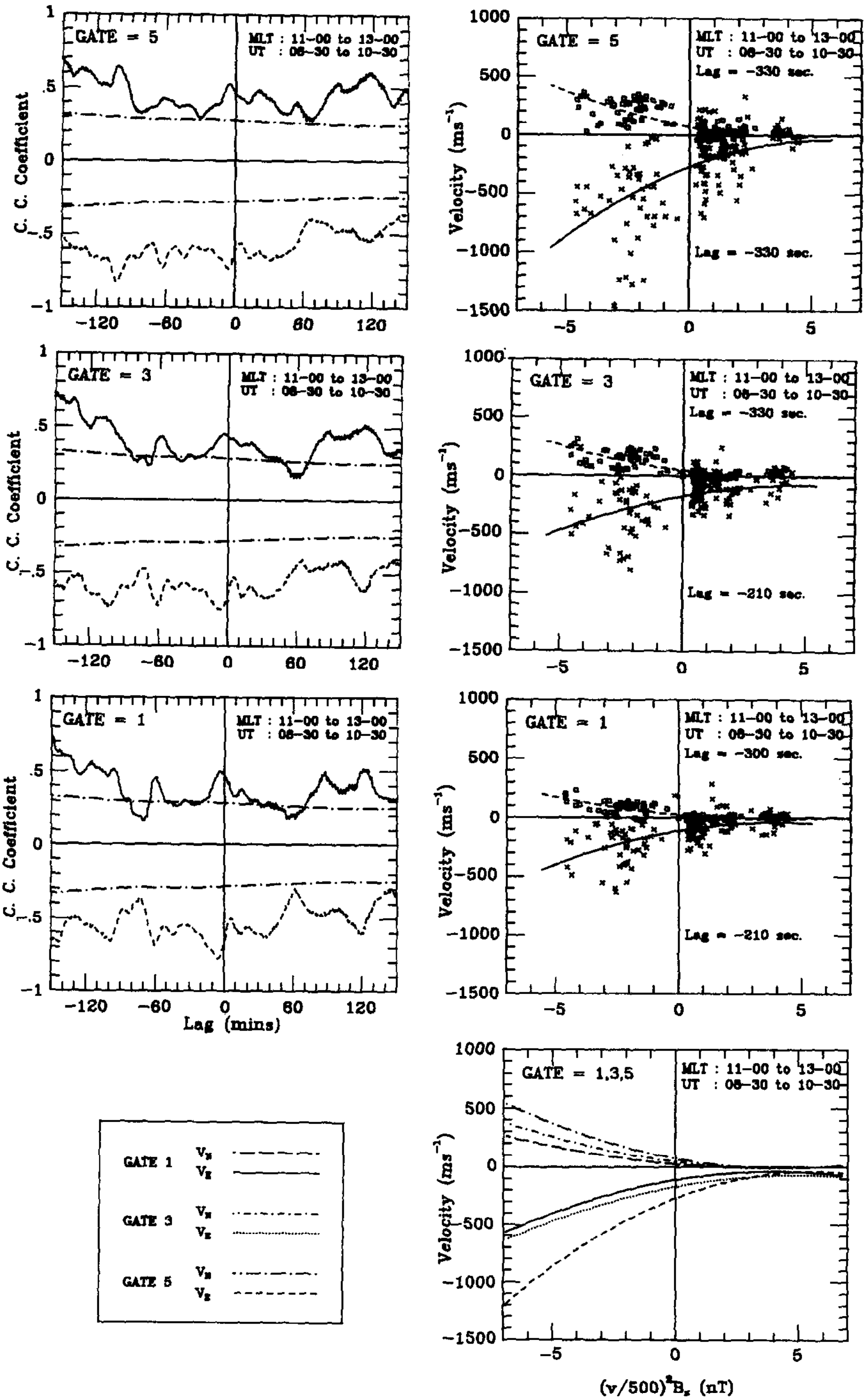

FIG. 4b. AS FOR FIG. 4a EXCEPT FOR THE LOCAL TIME INTERVAL FROM 11:00 TO 13:00 M.L.T.

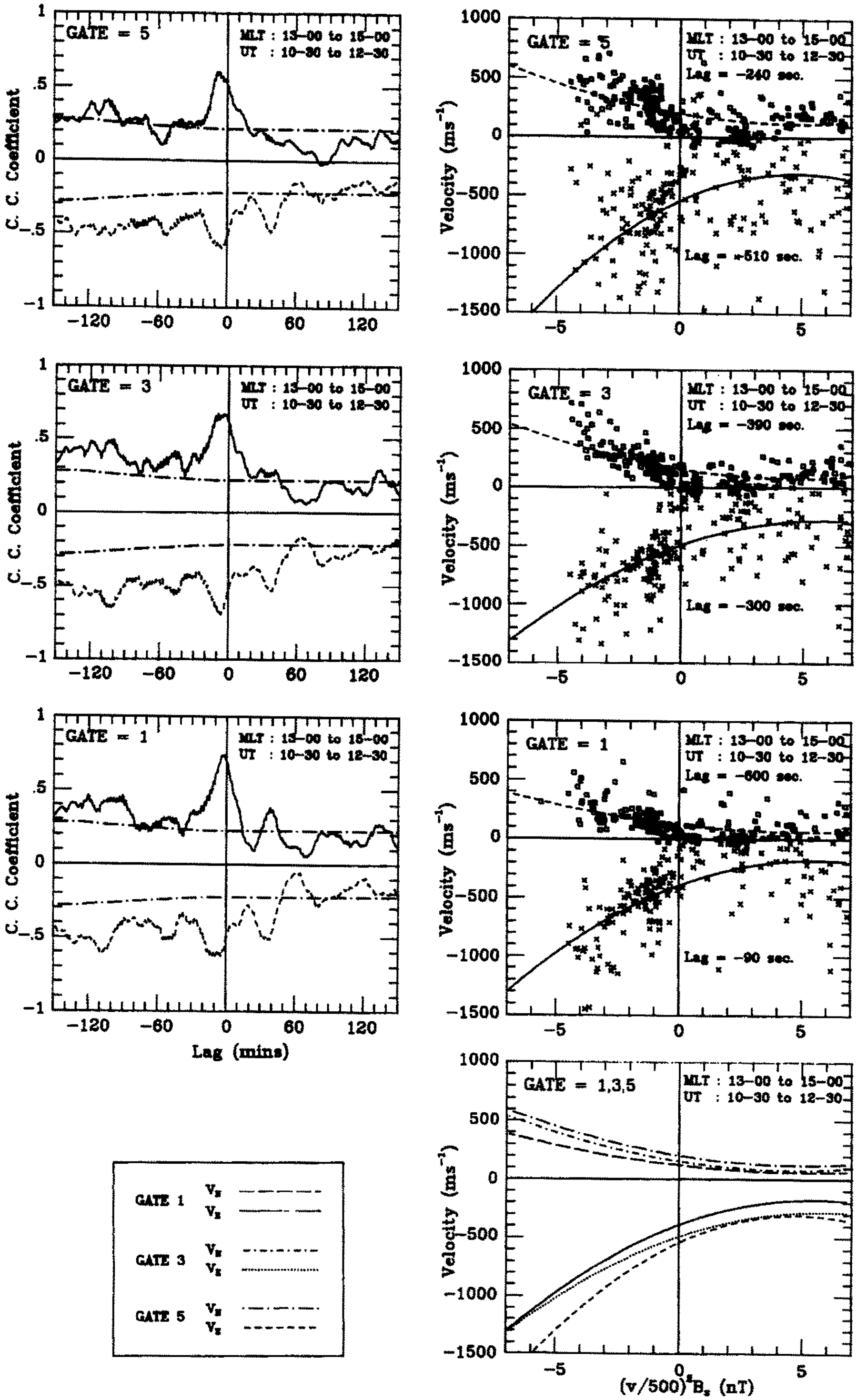

FIG. 4c. AS FOR FIG. 4a EXCEPT FOR THE LOCAL TIME INTERVAL FROM 13:00 TO 15:00 M.L.T.

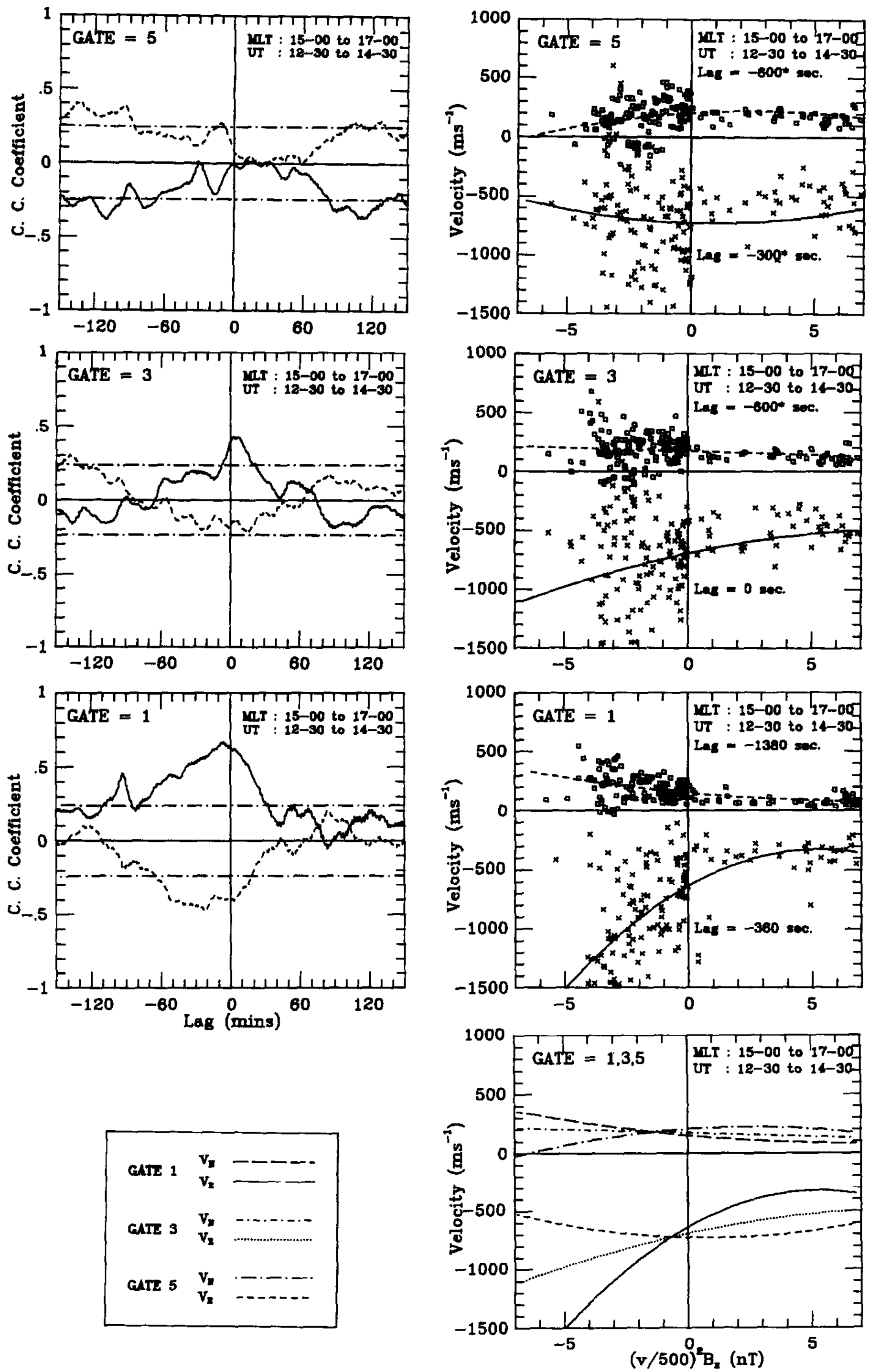

FIG. 4d. AS FOR FIG. 4a EXCEPT FOR THE LOCAL TIME INTERVAL FROM 15:00 TO 17:00 M.L.T.

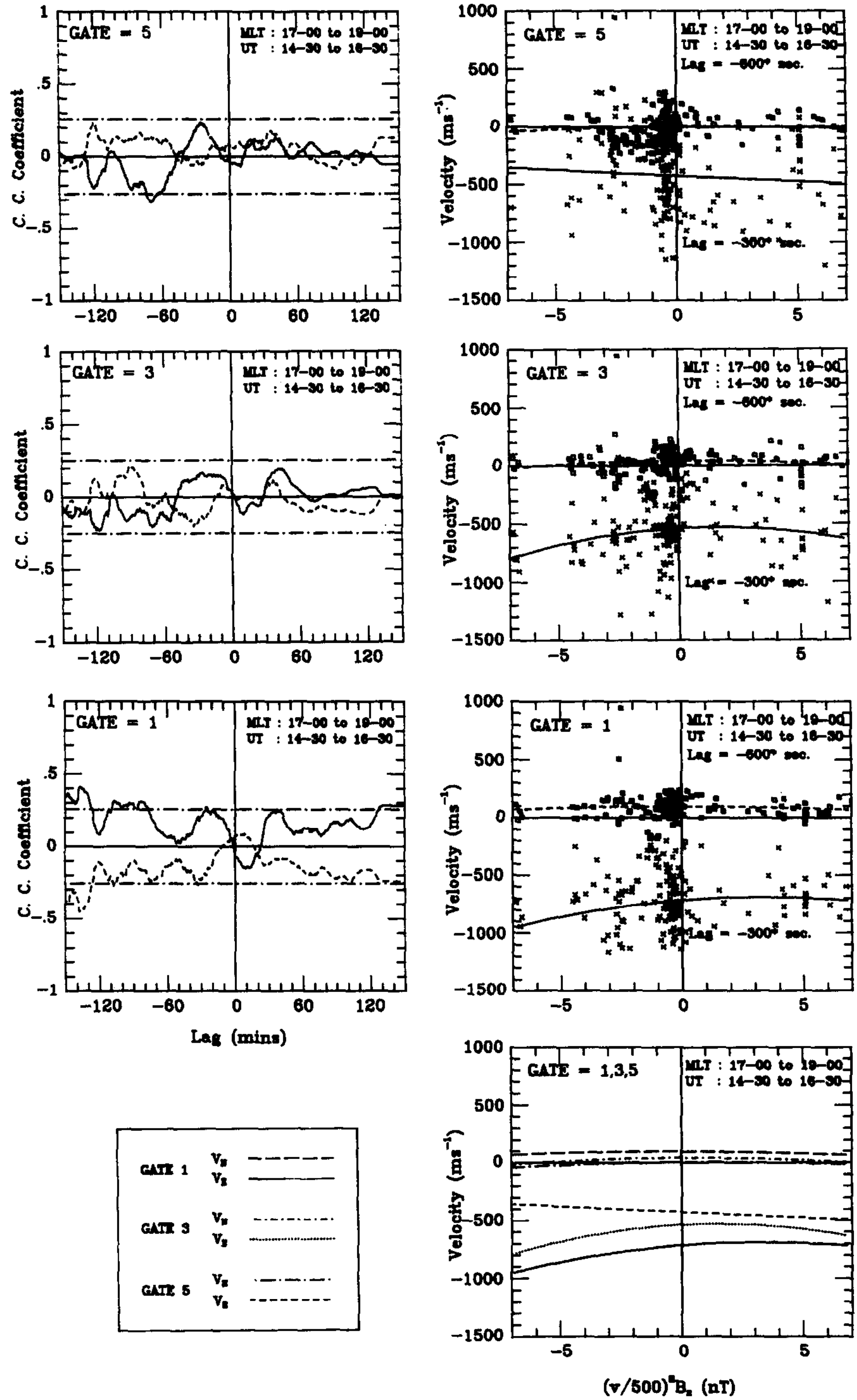

FIG. 4e. AS FOR FIG. 4a EXCEPT FOR THE LOCAL TIME INTERVAL FROM 17:00 TO 19:00 M.L.T.

gate 1, while for negative B_z it is lower. This result shows that gate 3 now lies between the peaks in the "most expanded" and "most contracted" cells. Correspondingly, the data also show a reduced response to B_z, as in graph (c) of Fig. 3. The data for gate 5, however, show that the modest steady flows which are again present for positive B_z (at values somewhat larger than in gates 1 and 3), give way to very mixed and variable values when B_z is negative. The new feature, compared e.g. with the data for gate 1, is the appearance of increasing numbers of low values of the flow components as B_z becomes increasingly negative. The average values, indicated by the fitted lines, now show a decline in both V_N and V_E as B_z becomes negative. Note that the correlation coefficients have correspondingly changed sign, though due to the scatter in the data no marked peaks occur above the 99.9% significance level in the correlograms. The data in this gate thus indicate a location close to the "cross-over" point where, as shown in graph (d) of Fig. 3, there is little response of the flow to B_z. As will be shown below, this gate also lies near the peak of the "most contracted" cell in this local time sector, such that the relationship between the location of this peak and the "cross-over" point, is, in fact, close to that depicted in the upper part of Fig. 3. In summary, therefore, in this local time sector gate 1 lies near the peak in the "most expanded" cell, gate 5 lies close to the peak of the "most contracted" cell which is approximately colocated with the "cross-over" point, while gate 3 lies mid-way between the peaks. The response of the flow in the three gates then corresponds to graphs (b), (c) and (d) in Fig. 3.

In Fig. 4e we finally show results for the 2 h interval centred on 18:00 M.L.T. Here the data are very scattered, giving rise to no obvious and convincing peaks in the correlograms. The scatter plots, however, produced for the nominal lags, indicate that for the first time the flow speeds for positive B_z decrease with increasing latitude between gates 1 and 5, indicating a location poleward of the peak flow in the quiet-time dusk cell. The flow speed in gate 1 is, however, comparable to that found in gate 5 in the previous local time sector (Fig. 4d), indicating that the peak in the "most contracted" cell now lies in its vicinity. Correspondingly, there is little overall variation of the flow with B_z in gate 1, as expected for a location close to the "cross-over" point [graph (d) in Fig. 3]. The simple model in Fig. 3 would then predict a decrease in the flow speed with negative B_z in gates 3 and 5 [graph (e)]. In fact the data do show increasing numbers of flow measurements for negative B_z which are smaller than the mean speeds for positive B_z in these gates, especially for gate 5. However, there is a wide scatter in the data, resulting in little overall response to B_z, and only gate 5 shows weak anticorrelation.

Overall, the results described above amply justify and substantiate the conclusions reported previously, based mainly on visual inspection of the EISCAT/*AMPTE* data set, that strong correlations exist between high-latitude dayside ionospheric flows and the North–South component of the IMF. It has been shown, however, that the form of the correlation varies significantly over the local time interval for which data are available (~09:00 to ~19:00 M.L.T.), in a way which is readily understandable in terms of the location of the radar field-of-view relative to the quiet-time flow pattern and to the patterns of enhanced flow excited by coupling at the magnetopause when IMF B_z is negative. In the next section we will look in more detail at these flows by using the curves fitted to the scatter plots to examine the flow pattern for various fixed values of IMF B_z.

4. FLOW PATTERNS FOR FIXED VALUES OF IMF B_z

Vector flow observations from individual runs of incoherent scatter radar experiments are often presented in the form of M.L.T.–latitude polar dial plots, rather than in the rectangular format e.g. used here in Fig. 2. "Polar" dial plots of the 1984 EISCAT/*AMPTE* experiments which form part of the present study may, for example, be found in Willis *et al.* (1986) (their Figs 5–7). Such plots can clearly give a more accurate impression of the two-dimensional geometry of ionospheric flows, but it is then tempting to interpret them in terms of an instantaneous flow pattern. The results presented in the previous section show that such interpretations will almost always be invalid, due to the strong modulation of the flow by IMF B_z. For a single radar, dial plots of the flow perforce take 24 h to complete, while IMF B_z typically varies significantly on much shorter time scales (as on all the experiment days included in this study). Inevitably, therefore, dial plots produced on this basis will be substantially affected by the temporal variations in IMF B_z which happen to occur during the experiments, and cannot be taken to represent an instantaneous picture.

From the results presented in the previous section we can, however, attempt to reconstruct the flow pattern for a given IMF B_z value by using the quadratic lines fitted to the scatter plots. Rather than use separate lag values for each gate and M.L.T. sector determined from the peaks in the correlograms, we have here, for simplicity, adopted a fixed lag value, to be used for both V_N and V_E. The value adopted is 7 min (420 s), which will be shown in the next section to be representative of the data as a whole (see also Fig. 4). However, experimentation has shown that the results are not very sensitive to the exact value chosen, to within a few minutes, as may also be gauged from the width of the peaks in the correlograms shown in the last section. The results shown in Fig. 5 for $(V/500)^2B_z = 0$, ± 2 and ± 4 nT were determined from overlapping 2 h segments of data (as in Fig. 4) centred at half-hour intervals from 09:30 to 18:30 M.L.T., with data from different gates (from 1 to 7) being treated separately. No flows are plotted for a given M.L.T. value if the data for that interval do not encompass the IMF B_z value corresponding to the plot. Specifically, we do not extrapolate the quadratic curves fitted to the scatter plot data more than ± 1.5 nT beyond the maximum and minimum B_z values in that segment of data.

Turning now to the results in Fig. 5, we first consider the two flow maps for positive IMF B_z, these being taken together because of their close similarity. These flows correspond to the "most contracted" pattern in the above discussion, and it may be recalled that the scatter plots presented in the previous section show little variation with B_z when the latter is positive, such that the fitted lines are then, in the main, flat. (This lack of response to positive B_z was, of course, already implicit in our simple picture in Fig. 3.) The only significant exception to this statement occurs at the earliest local times for which data are available in this study, in the mid-morning sector, where differences can be seen between the maps shown for $B_z = 2$ and 4 nT (cf. also Fig. 4a). In this sector eastward flows are observed in the upper gates, corresponding to the equatorward region of the dawn auroral zone flow cell, which decline in strength with increasing local time as the cell recedes poleward across the field-of-view. These flows give way at later local times to the weak (typically 100 m s^{-1}) westward flows of the quiet-time noon sector (Fig. 4b), this process being essentially complete by $\sim$10:30 M.L.T. in the map for $B_z = 2$ nT. The transition from eastward to westward flows in the "Polar" data thus clearly takes place in the pre-noon hours. The time of the transition for $B_z = 4$ nT is obscured by the lack of large B_z data in the immediate pre-noon hours which results in the gaps in the corresponding vector plot at 10:30 and 11:00 M.L.T., but from the fact that the eastward flows observed prior to the gap are considerably larger for $B_z = 4$ nT than at the same M.L.T. for $B_z = 2$ nT, we may infer that the transition takes place at a later local time, nearer to noon, in the former case than in the latter. It thus appears that the East–West flow transition, while occurring consistently pre-noon in the data, occurs at earlier local times, nearer to dawn, as B_z falls in value. Examination of the results for zero and negative B_z, to be discussed further below, suggests that this shift continues, to $\sim$09:30 M.L.T. when IMF $B_z = 0$ nT, and into the early morning region (where data are unavailable) when IMF B_z is negative.

Looking now at the flow maps for $B_z = 2$ and 4 nT at later local times, the radar field-of-view remains equatorward of the main auroral zone flows from $\sim$10:30 to $\sim$13:00 M.L.T., after which the westward flows of the quiet-time dusk cell appear (in accordance with the previous discussion of Fig. 2). The peak in the dusk cell flow, where the speed maximizes at $\sim$1 km s^{-1}, crosses the field-of-view from the most poleward to the most equatorward gate between 15:00 and 18:00 M.L.T. Thus, in the "Polar" field-of-view, flow speeds increase monotonically with latitude before 15:00 M.L.T., and decrease monotonically with latitude after 18:00 M.L.T., as noted in the discussion of Fig. 4. Between these times the peak in the flow speed occurs within the field-of-view so that the variation of the observed speeds with latitude becomes relatively small. The peak lies in the vicinity of gate 5 at 16:00 M.L.T. and near gate 1 at 18:00 M.L.T., in conformity with the discussion of Figs 4d and 4e.

When IMF B_z is near zero or negative, however, substantial changes in the flow pattern are clearly evident in Fig. 5. These can be discussed in terms of three main effects. The first is the local time shift of the dayside East–West flow reversal into the early morning hours discussed above. This effect results in the appearance of westward flows at all local times for which data are available, extending from dusk into the mid-morning hours. The second effect is a large equatorward expansion of the flow pattern, including an inferred expansion in the size of the polar cap (cf. Fig. 3). This effect, taken together with the first, results in the appearance of B_z-modulated north-westward directed flows throughout the noon sector, which replace the weak ($\sim$100 m s^{-1}) latitude-independent westward drifts observed in this sector for positive IMF B_z. The expansion effect also results in the centre of the dusk flow cell being traversed significantly earlier in local time for negative than for positive IMF B_z. In the map for $B_z = -4$ nT, for example, the peak in the flow speed moves equatorward across the field-of-view between 13:00 and 16:00 M.L.T., such that flow speeds increase monotonically with latitude before the former time, and decrease monotonically with latitude after the latter. Note that these numbers indicate that the peak of the "most expanded" cell lies near gate 5 at 14:00 M.L.T. and near gate 1 at 16:00 M.L.T., in conformity with the discussion of Figs 4c and 4d. For B_z positive the corresponding times are

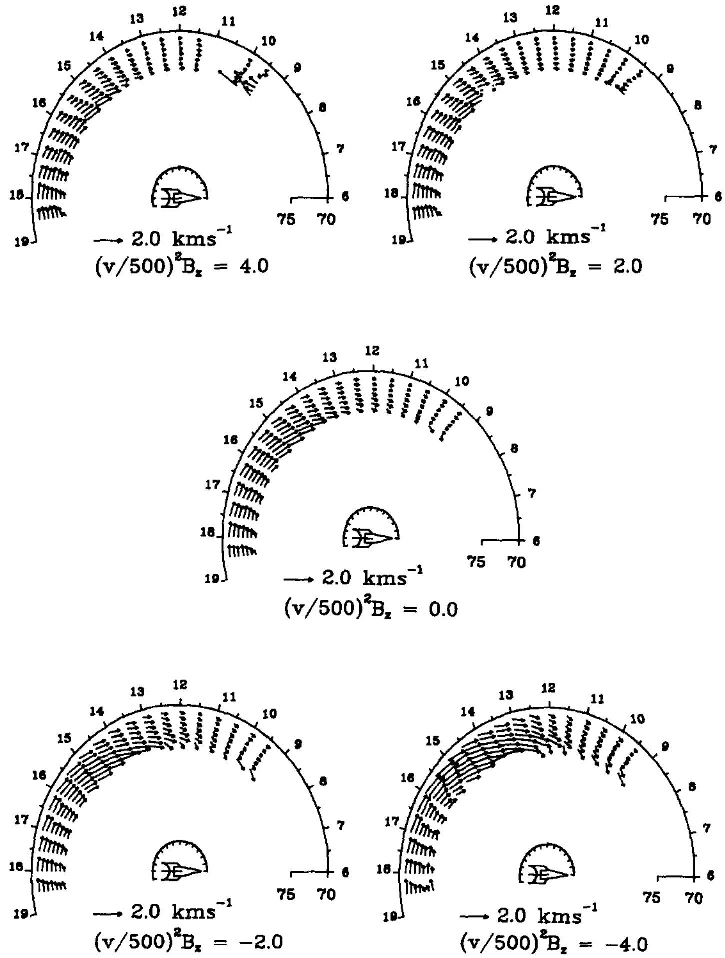

FIG. 5. VECTOR FLOWS DETERMINED FROM THE "POLAR" DATA ARE SHOWN IN M.L.T.–LATITUDE POLAR DIAL FORMAT FOR FIXED VALUES OF $(V/500)^2B_z$ (viz. 0, ± 2 nT AND ± 4 nT).

These were determined from overlapped 2 h M.L.T. segments of the data computed every half hour for each gate (from 1 to 7) separately, by using least-squares quadratic fits to the data (as in Fig. 4). For simplicity a constant lag time of 7 min between (shifted) IMF B_z values and ionospheric velocity values has been employed. Latitude profiles of the flow are not shown for a given M.L.T. sector and B_z value if the data from that sector do not extend to that B_z value (to within a margin of 1.5 nT).

15:00 and 18:00 M.L.T., such that this feature has shifted 2 h in local time between the maximum and minimum B_z values. This effect accounts for the dependence of the latitudinal gradient of the flow on B_z found in Fig. 4, as previously discussed. Flows increase with latitude (across gates 1–5) over the whole range of B_z values encountered in our study at 12:00 and 14:00 M.L.T. (Figs 4b and 4c), decrease with latitude for all B_z at 18:00 M.L.T. (Fig. 4e), while the gradient reverses in sense as B_z changes from positive to negative at 16:00 M.L.T. (Fig. 4d).

These results also give the relevant information required to define the spatial region where strong positive correlations are found between the flow speed and IMF B_z. It will be recalled from Fig. 4 that strong correlations are generally confined to the region equatorward of the mid-point between the peaks of the "most expanded" and "most contracted" cells. Poleward of the mid-way point only weak correlations and much scatter are evident in the data, for reasons already discussed. From the above results, the mid-way point crosses the "Polar" field-of-view between 14:00 (gate 7) and 17:00 M.L.T. (gate 1). Thus, for example, strong correlations are observed from the pre-noon hours until 14:00 M.L.T. in gate 7, 15:00 M.L.T. in gate 5, 16:00 M.L.T. in gate 3 and 17:00

M.L.T. in gate 1 (see Fig. 4). These results therefore define the limits of the region from which flow response times can be determined from the data, as will be discussed further in the following section.

The third and final factor to be considered in Fig. 5 is the overall increase in the magnitude of the flow speeds which are observed for increasingly negative B_z, typified by the enhancement of the peak flow speed in the dusk cell from ~ 1 km s^{-1} when $B_z = +4$ nT to ~ 1.5 km s^{-1} when $B_z = -4$ nT. It may be noted from the discussion in Section 2 that it is the presence of this factor which results in the strong positive correlations between flow speed and IMF B_z in the region equatorward of the cross-over point, and the much flatter responses poleward of this point which are observed in Fig. 4. Given just an expansion in the flow pattern, but no increase in overall flow speed, we would have expected the anticorrelation between the flow and B_z poleward of the "cross-over" point to have been approximately equal in significance to the positive correlation occurring in the equatorward region. Instead, the enhancements in flow speed add to the positive correlations equatorward of the cross-over point but subtract from the anticorrelations poleward thereof, thus giving rise to a much stronger effect in the former than in the latter region.

In conclusion we note that owing to the rather restricted latitude and local time coverage of the joint EISCAT "Polar"/*AMPTE* data set analysed here, the results presented in this section represent only a modest contribution to an understanding of high latitude flows and their dependence on interplanetary parameters. However, the results do convincingly demonstrate the potential of radar data to derive detailed maps of high-latitude flows which occur under different IMF conditions, by suitably combining data from several experiments. In the future it should be possible to extend our results in local time using the data from subsequent "Polar" runs, and also extend them in latitude, by using modified experiments run on the EISCAT radar, together with data acquired from other radar systems. With a larger data set it should also be possible to look for more subtle effects in the flow data, such as dependences on the components of the IMF in the equatorial plane.

5. IONOSPHERIC RESPONSE TIME

In this section we provide further details of the results concerning the response time of the ionosphere to changes in the North–South component of the IMF. These are determined from the lag times of the peaks in the correlograms between the flow components V_N and V_E, and V^2B_S. However, we note that the occurrence of such peaks is confined to the region equatorward of the mid-way point between the "most expanded" and "most contracted" flow patterns in the data set, and therefore that it is only in this region that the response time can be reliably determined. Explicitly, results for V_N are obtained from the earliest local times available ($\sim$10:00 M.L.T.) until 17:00 M.L.T. in gate 1, 16:00 M.L.T. in gate 3, 15:00 M.L.T. in gate 5 and 14:00 M.L.T. in gate 7. At later local times the relative lack of response of the flow to IMF B_z results in correlograms with no consistent peak, as seen previously in Fig. 4. Results for V_E are further restricted by the lack of strong response of this component in the vicinity of the East–West flow reversal, such that significant peaks do not occur in the V_E correlograms until after $\sim$10:30 M.L.T. (cf. Fig. 4a).

One of the points made above, arising from both visual inspection of the data shown in Fig. 2 and from the correlograms in Fig. 4, is that within a given M.L.T. sector there appears to be no systematic variation in the ionospheric response delay with latitude across the "Polar" field-of-view. This topic is further investigated in Fig. 6, where we show the delay vs gate number (spanning the latitude range 70.8°–74.3° from gates 1 to 7) for three non-overlapping 2 h local time sectors, centred on 10:00, 12:00 and 14:00 M.L.T. (Later M.L.T. intervals are not displayed due to the restrictions noted above, remembering that the "mid-way" point appears in gate 7 at 14:00 M.L.T. and has reached gate 3 by 16:00 M.L.T.) Squares and triangles show the response times of V_N and V_E, respectively, and the error bars are obtained from a visual estimate of how well the position of the peaks in the correlograms can be determined. The points plotted correspond only to well-defined peaks in the correlograms which are above the 99.9% significance level and are consistently present from sector-to-sector and gate-to-gate.

In can be seen from Fig. 6 that, overall, there are no systematic variations of the response time with latitude in each of the three M.L.T. sectors shown. There is some indication of an increase in the response time of V_E with latitude at 12:00 and 14:00 M.L.T., though the variation is probably not significant within the estimated errors. The overall lack of latitudinal dependence is consistent with the finding in Section 2 that following changes in the North–South component of the IMF, the flows appropriate to the new value are established coherently in time across the whole "Polar" field-of-view. It can also be seen, however, that variations do occur with M.L.T. At 10:00 M.L.T. the average response time for V_N is 11.0 ± 1.6 min (see Fig. 4a and associated discussion), decreasing to 5.6 ± 0.6 and 6.6 ± 1.9 min at 12:00 and 14:00

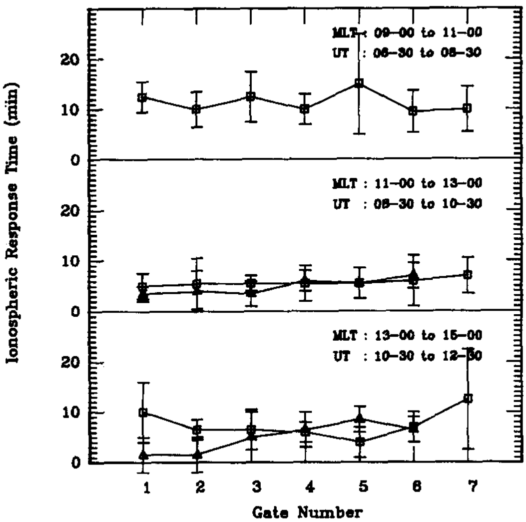

FIG. 6. THE IONOSPHERIC RESPONSE TIME TO CHANGES IN THE NORTH–SOUTH COMPONENT OF THE IMF IS SHOWN VS LATITUDE (GATE NUMBER) FOR THREE NON-OVERLAPPING 2 h SECTORS OF LOCAL TIME, CENTRED ON 10:00, 12:00 AND 14:00 M.L.T.

Squares refer to V_N and triangles to V_E. These times were determined from the peaks in the corresponding correlograms, with error bars determined from a visual estimate of how precisely the position of the peak could be determined. Only well-defined peaks above the 99.9% significance level which are consistently present from sector-to-sector and gate-to-gate are included.

M.L.T. (see Figs 4b and 4c). (The values given here are the averages and standard deviations of the data shown in Fig. 6, weighted in proportion to the inverse of the estimated error.) The response times for V_E at 12:00 and 14:00 M.L.T. are 4.9 ± 1.4 and 5.2 ± 2.7 min, both being smaller than the corresponding values for V_N, though perhaps not significantly so given the estimated uncertainties. Averaging together the five response times given above then yields an overall value of 6.7 min, thus substantiating the use of 7 min in the production of the flow maps presented in Fig. 5. The weighted gate-averaged response times and their standard deviations for each 2-h interval centred on integer M.L.T. hours are given in Table 3.

TABLE 3

M.L.T. sector (± 1 h)	V_N response time (min)	V_E response time (min)
1000	11.0 ± 1.6	—
1100	7.2 ± 1.5	—
1200	5.6 ± 0.6	4.9 ± 1.4
1300	8.7 ± 2.4	3.0 ± 0.9
1400	6.6 ± 1.9	5.2 ± 2.7
1500	6.6 ± 2.4	2.3 ± 2.4

The local time dependence of the ionospheric response delay is explored in greater detail in Fig. 7, where we show the delay for gates 1, 3 and 5 vs M.L.T., in a format similar to that employed in Fig. 6. The M.L.T. coverage in each gate again reflects the restrictions in these data discussed above. Results are shown for overlapped 2 h segments of data computed every half hour. It can be seen that the response times are fairly constant in the noon to mid-afternoon sector ($\sim$12:00 to $\sim$15:00 M.L.T.), where the radar field-of-view lies within (or just equatorward of) the equatorward and central portions of the quiet-time dusk cell. Here the response time for V_E is 3.9 ± 2.2 min, but is again somewhat larger for V_N at 6.7 ± 2.2 min. These numbers were obtained from the weighted response times centred at integer hourly M.L.T. values from 12:00 to 15:00 M.L.T. inclusive, with values from all gates being included. At earlier local times the response times for V_N and V_E are nearly equal in the lower gates, and tend to increase with decreasing local time to 11 min at 10:00 M.L.T., as noted above. At later local times, nearer to dusk, the response times in the lower gates again increase, to $\sim$10 min for V_E and $\sim$20 min for V_N.

The principal conclusion arising from these results is that changes in flow occur very promptly in the dayside ionosphere in response to variations in the North–South component of the IMF. About 4 min after a southward turning of the IMF appears at the magnetopause, flows are excited within the "Polar" field-of-view which are westward directed in the early afternoon sector, turning to north-westward at noon. However, the longer response delays which occur at earlier and later local times, and in the early afternoon V_N results, show that the flow pattern must evolve in form over a $\sim$5 min interval following the initial excitation. In particular, north-westward flows appear to continue to grow in the mid-morning hours, possibly as a result of a shift in the location of the morning East–West flow reversal occurring on these time scales, and the early afternoon flows rotate in direction from westward to north-westward as previously noted in Section 3. The latter effect could result from a distortion in shape of the polar cap region, if a bulge of open flux is temporarily produced in the dayside ionosphere by enhanced reconnection at the magnetopause. This would have the effect of reducing the northward tilt of the afternoon auroral zone "return" flows, until the boundary resumes a more usual orientation as the open flux redistributes itself. Clearly these remarks are speculative, and further clarification is required of how the dayside flows evolve following rapid changes in the IMF direction. To this end, it will be necessary to undertake further case studies of

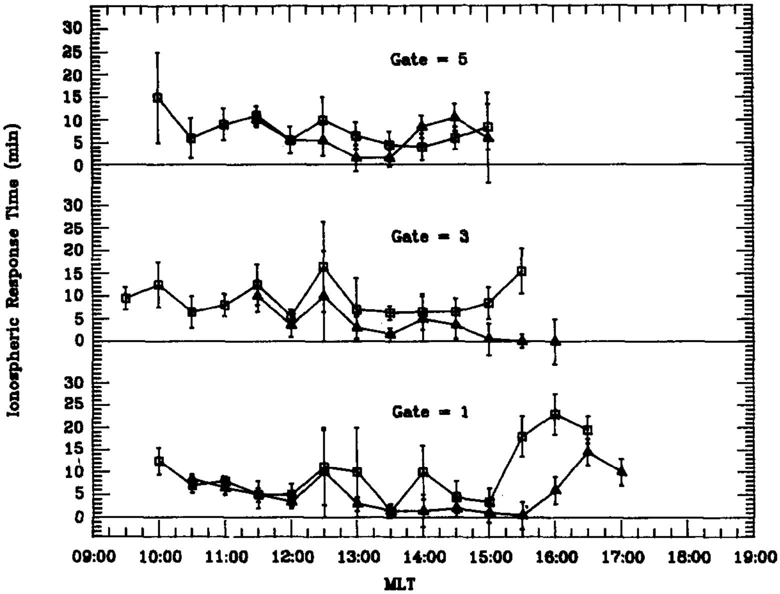

FIG. 7. THIS FIGURE HAS A SIMILAR FORMAT TO FIG. 6, BUT SHOWS THE RESPONSE TIME VS M.L.T. FOR GATES 1, 3 AND 5.
Values are shown every half hour determined from overlapping 2 h segments of data.

the ionospheric response to abrupt changes in the IMF in different M.L.T. sectors.

6. SUMMARY

In 1984 and 1985 a series of five experiments was undertaken in which ionospheric flows were measured by the EISCAT "Polar" experiment, while observations of the solar wind and IMF were made upstream of the Earth's bow shock by the *AMPTE UKS* and *IRM* spacecraft. The "Polar" data provide a 7-point profile of the ionospheric flow between 70.8° and 74.3° invariant latitude every 2.5 min, with the data acquired simultaneously with *AMPTE* (totalling 40 h) covering the dayside local time sector from ~09:30 to ~18:30 M.L.T. This data set therefore refers principally to the region of the morningside East–West flow reversal and the "dusk" auroral zone flow cell. Relatively little information has been obtained about the properties of the dawn flow cell in this study. Previous papers have presented examples of apparent correlations between these data sets, specifically between the flows and the North–South component of the IMF, principally from visual inspection of the data (Rishbeth *et al.*, 1985; Todd *et al.*, 1988). The aim of the present paper has been to establish quantitatively whether statistically significant relationships exist for the data set as a whole, and, if so, to determine both the form of the ionospheric flow response to IMF B_z and the time scales involved. To this end the two components of ionospheric flow (northward and eastward) have been cross-correlated with the interplanetary half-wave rectifier function V^2B_S (where V is the solar wind speed and B_S is the southward field component). The latter function was chosen after a preliminary analysis showed that it tends to give higher peak cross-correlation coefficients than the other parameters which were tried (which included B_z, B_S, VB_S, ε etc.). The detailed form of the flow response was then examined by forming scatter plots of the "Polar" data vs V^2B_z, using the lag time corresponding to the peak in the corresponding correlogram, and then fitting quadratic curves through the data.

This analysis has shown that the behaviour of the correlograms, and the corresponding relationships between the ionospheric flow components and IMF B_z, depends strongly on both latitude and local time. Clear, statistically significant, correlation peaks well above the 99.9% significance level, which correspond to strong IMF B_z dependence of the flows, are observed in some regions, but only small correlations, corresponding to scattered data and little IMF dependence, are observed in others. Specifically, at any given latitude within the "Polar" field-of-view a strong positive correlation between the westward "dusk cell" flow and negative IMF B_z is observed in the noon and early afternoon sectors. At later local times nearer to dusk the correlations become successively weaker (and the data correspondingly more scattered and exhibiting less B_z dependence), until eventually weak anti-correlation between the westward flow and IMF B_z is observed (at least in the more poleward of the EISCAT gates). This pattern of behaviour occurs at successively earlier local times with increasing latitude, the appearance of weak correlations occurring e.g. in gate 7 (73.4°) at ~14:00 M.L.T., compared with ~17:00 M.L.T. in gate 1 (70.8°). It has been shown that these results can be explained in terms of a simple model in which the magnitude and latitudinal extent of the flows becomes successively larger as B_z becomes successively more negative. These features of the response have been confirmed by deriving detailed flow maps for various B_z values from the scatter-plot data. At the simplest level, the strong positive correlations are observed in the equatorward portions of the flow cells where both effects mentioned above combine to produce large increases in flow speed with negative B_z. The equatorward portions of the cells are observed in the "Polar" field-of-view at sufficiently early local times, but due to the nightside offset between the centre of the polar cap and the magnetic pole, the field-of-view moves into the poleward portions of the flow cells at later local times (successively later at successively lower latitudes). In the poleward region, anticorrelation occurs between the flow and IMF B_z due to the equatorward shift of the flow pattern arising from the expansion of the polar cap with negative B_z. However, this effect is by no means as great as the positive correlation observed in the equatorward portions of the cell because it is offset by the overall increase in flow speed (rather than being augmented by the latter, as in the equatorward region). It is only in the equatorward portions of the cells, therefore, that clear peaks in the correlograms are obtained.

As a consequence of these effects, the data which can be used to investigate the ionospheric response time to IMF changes are restricted, but nevertheless a number of important results have been obtained. It has firstly been found that no significant latitudinal dependence in response time is present in the data, thus confirming previous suggestions, based upon visual inspection, that flow changes take place coherently across the radar field-of-view, with no noticeable lag from gate-to-gate. However, variations do occur with local time. The most rapid response is observed in the noon to mid-afternoon sector, where the westward flows of the dusk cell respond to the direction of the magnetosheath field at the subsolar magnetopause with a delay of only 3.9 ± 2.2 min. This response is very fast, but is nevertheless rather longer than the Alfven-wave transit time between the equatorial magnetopause and the ionosphere. This transit time is well known for the "Polar" field-of-view from the characteristic period of ULF pulsations which are often observed in the data in the dayside ionosphere (Todd *et al.*, 1988). Assuming that the oscillation represents a standing wave in the fundamental mode, the typical wave periods of ~4 min represent the Alfven wave travel time between one hemisphere to the other, and back again. The Alfven wave transit time between the equator and the ionosphere on these field lines is then no more than ~1 min, and although the "Polar" field-of-view is generally located on closed field lines equatorward of the dayside cusp, the transit time in the vicinity of the latter can hardly be very different. The rather longer flow response times found here may then contain contributions from other factors, such as the time taken for coupling processes to be initiated at the magnetopause (though we know of no reason why this should be significant), the "impedance mismatch" between the magnetosphere and ionosphere which may require several Alfven wave transits between the magnetopause and ionosphere to establish ionospheric flow, and the time taken for the ionospheric effects to expand from their initial point of contact with the ionosphere to the "Polar" field-of-view in the manner described by Lockwood *et al.* (1986b).

It may be recalled from the Introduction that rapid, few minute responses have previously been reported for the excitation of the DP-2 current system following southward turnings of the IMF, and we would relate our results directly to those. Our results clearly bear no relation to the ~45 min delays typically found for the response of magnetic disturbance indices such as AE or AL to IMF B_z. These latter parameters must therefore be responding to a different characteristic time scale of the coupled solar wind–magnetosphere–ionosphere system (i.e. the time scale for the onset of the substorm instability in the geomagnetic tail). However, longer response times are observed in our data in earlier and later local time sectors, and in V_N relative to V_E in the early afternoon sector. These results suggest that after the initial excitation of the ionospheric flow on the above time scales, the flow continues to evolve in form over the following ~5 min, as the system accommodates to the new boundary conditions. Further case studies need to be undertaken to establish the details of how dayside flows are excited and subsequently evolve following sudden changes in the IMF.

Acknowledgements—We thank the Director and staff of EISCAT for their help, Dr G. Paschmann for the provision of *AMPTE IRM* plasma data, Prof. D. J. Southwood for the provision of *AMPTE UKS* magnetometer data and Dr W. A. C. Mier-Jedrzejowicz for aid in the processing of the latter. EISCAT is supported by the British SERC, French CNRS, West German MPG, Norwegian NAVF, Swedish NFR and Finnish SA. *AMPTE* is a collaborative project of NASA (U.S.A.), DFVLR and MPG (West Germany) and the SERC (U.K.). AE was supported by a SERC Research Assistantship.

REFERENCES

Akasofu, S.-I., Carbary, J. F., Meng, C.-I., Sullivan, J. P. and Lepping, R. P. (1982) A high time resolution study of the solar wind–magnetosphere energy coupling function. *Planet. Space Sci.* **30**, 537.

Alcayde, D., Caudal, G. and Fontanari, J. (1986) Convection electric fields and electrostatic potential over $61° < \lambda < 72°$ invariant latitude observed with the European incoherent scatter facility: initial results. *J. geophys. Res.* **91**, 233.

Arnoldy, R. L. (1971) Signature in the interplanetary medium for substorms. *J. geophys. Res.* **76**, 5189.

Baker, D. N., Hones, E. W., Jr., Payne, J. B. and Feldman, W. C. (1981) A high-time resolution study of interplanetary parameter correlations with *AE. Geophys. Res. Lett.* **8**, 179.

Baker, D. N., Zwikl, R. D., Bame, S. J., Hones, E. W., Jr., Tsurutani, B. T., Smith, E. J. and Akasofu, S.-I. (1983) An *ISEE* 3 high time resolution study of interplanetary parameter correlations with magnetospheric activity. *J. geophys. Res.* **88**, 6230.

Bargatze, L. F., Baker, D. N., McPherron, R. L. and Hones, E. W., Jr. (1985) Magnetospheric impulse response for many levels of geomagnetic activity. *J. geophys. Res.* **90**, 6387.

Baumjohann, W. and Haerendel, G. (1985) Magnetospheric convection observed between 06:00 and 21:00 L.T.: solar wind and IMF dependence. *J. geophys. Res.* **90**, 6370.

Baumjohann, W., Nakamura, R. and Haerendel, G. (1986) Dayside equatorial-plane convection and IMF sector structure. *J. geophys. Res.* **91**, 4557.

Berchem, J. and Russell, C. T. (1984) Flux transfer events on the magnetopause: spatial distribution and controlling factors. *J. geophys. Res.* **89**, 6689.

Bryant, D. A., Krimigis, S. M. and Haerendel, G. (1985) Outline of the *Active Magnetospheric Particle Tracer Explorers* (*AMPTE*) mission. *IEEE Trans. Geosci. Remote Sensing* **GE-23**, 177.

Burch, J. L., Reiff, P. H., Menietti, J. D., Heelis, R. A., Hanson, W. B., Shawhan, S. D., Shelley, E. G., Sugiura, M., Wiemer, D. R. and Winningham, J. D. (1985) IMF B_y dependent plasmaflow and Birkeland currents in the dayside magnetosphere: *Dynamics Explorer* observations. *J. geophys. Res.* **90**, 1577.

Burton, R. K., McPherron, R. L. and Russell, C. T. (1975) An empirical relationship between interplanetary conditions and D_{st}. *J. geophys. Res.* **80**, 4204.

Clauer, C. R. and Banks, P. M. (1986) Relationship of the interplanetary electric field to the high-latitude ionospheric electric field and currents: observations and model simulation. *J. geophys. Res.* **91**, 6959.

Clauer, C. R., Banks, P. M., Smith, A. Q., Jorgensen, T. S., Friis-Christensen, E., Vennerstrom, S., Wickwar, V. B., Kelly, J. D. and Doupnik, J. (1984) Observation of IMF and ionospheric plasma convection in the vicinity of the dayside polar cleft. *Geophys. Res. Lett.* **11**, 891.

Clauer, C. R. and Kamide, Y. (1985) DP 1 and DP 2 current systems for the March 22, 1979 substorms. *J. geophys. Res.* **90**, 1343.

Clauer, C. R., McPherron, R. L., Searls, C. and Kivelson, M. G. (1981) Solar wind control of auroral zone geomagnetic activity. *Geophys. Res. Lett.* **8**, 915.

Cowley, S. W. H. (1980) Plasma populations in a simple open model magnetosphere. *Space Sci. Rev.* **25**, 217.

Cowley, S. W. H. (1981) Magnetospheric asymmetries associated with the *Y*-component of the IMF. *Planet. Space Sci.* **29**, 79.

Cowley, S. W. H. (1982) The causes of convection in the Earth's magnetosphere: a review of developments during the IMS. *Rev. Geophys. Space Phys.* **20**, 531.

Cowley, S. W. H. (1983) Interpretation of observed relations between solar wind characteristics and effects at ionospheric altitudes, in *High Latitude Space Plasma Physics* (Edited by Hultqvist, B. and Hagfors, T.), p. 225. Plenum Press, New York.

Cowley, S. W. H. (1984) Solar wind control of magnetospheric convection. *Proc. Conf. Achievements of the IMS*. ESA SP-217, p. 483.

Cowley, S. W. H. (1986) The impact of recent observations on theoretical understanding of solar wind–magnetosphere interactions. *J. Geomagn. Geoelect.* **38**, 1223.

Doupnik, J R., Banks, P. M., Baron, M. J., Rino, C. L. and Petriceks, J. (1972) Direct measurements of plasma drift velocities at high magnetic latitudes. *J. geophys. Res.* **77**, 4268.

Doyle, M. A. and Burke, W. J. (1983) S3-2 measurements of the polar cap potential. *J. geophys. Res.* **88**, 9125.

Dungey, J. W. (1961) Interplanetary field and the auroral zones. *Phys. Rev. Lett.* **6**, 47.

Evans, J. V., Holt, J. M., Oliver, W. L. and Wand, R. H. (1980) Millstone Hill incoherent scatter observations of auroral convection over $60° < \lambda < 75°$: initial results. *J. geophys. Res.* **85**, 41.

van Eyken, A. P., Rishbeth, H., Willis, D. M. and Cowley, S. W. H. (1984) Initial EISCAT observations of plasma convection at invariant latitudes 70°–77°. *J. atmos. terr. Phys.* **46**, 635.

Fairfield, D. H. (1971) Average and unusual locations of the Earth's magnetopause and bow shock. *J. geophys. Res.* **76**, 6700.

Fontaine, D., Perraut, S., Alcayde, D., Caudal, G. and Higel, B. (1986) Large scale structures of the convection inferred from coordinated measurements by EISCAT and *GEOS* 2. *J. atmos. terr. Phys.* **48**, 973.

Formisano, V. (1979) Orientation and shape of the Earth's bow shock in three dimensions. *Planet. Space Sci.* **27**, 1151.

Formisano, V., Domingo, V. and Wenzel, K.-P. (1979) The three-dimensional shape of the magnetopause. *Planet. Space Sci.* **27**, 1137.

Foster, J. C. (1983) An empirical electric field model derived from Chatanika radar data. *J. geophys. Res.* **88**, 981.

Foster, J. C., Banks, P. M. and Doupnik, J. R. (1982) Electrostatic potential in the auroral ionosphere derived from Chatanika radar observations. *J. geophys. Res.* **87**, 7513.

Foster, J. C. and Doupnik, J. R. (1984) Plasma convection in the vicinity of the dayside cleft. *J. geophys. Res.* **89**, 9107.

Foster, J. C., Doupnik, J. R. and Stiles, G. S. (1981) Large-scale patterns of auroral ionospheric convection observed with the Chatanika radar. *J. geophys. Res.* **86**, 11357.

Heelis, R. A. (1984) The effects of the interplanetary magnetic field orientation on dayside high-latitude ionospheric convection. *J. geophys. Res.* **89**, 2873.

Heelis, R. A., Foster, J. C., de la Beaujardiere, O. and Hall, J. (1983) Multistation measurements of high-latitude ionospheric convection. *J. geophys. Res.* **88**, 10111.

Heelis, R. A. and Hanson, W. B. (1980) High-latitude ion convection vectors in the night time *F*-region. *J. geophys. Res.* **85**, 1995.

Heppner, J. P. (1972) Polar cap electric field distributions related to the interplanetary magnetic field direction. *J. geophys. Res.* **27**, 4877.

Heppner, J. P. (1973) High-latitude electric fields and modulations related to interplanetary magnetic field parameters. *Radio Sci.* **8**, 933.

Heppner, J. P. (1977) Empirical models of high latitude electric fields. *J. geophys. Res.* **82**, 1115.

Heppner, J. P. and Maynard, N. C. (1987) Empirical high-latitude electric field models. *J. geophys. Res.* **92**, 4467.

Holzer, R. E. and Slavin, J. A. (1979) A correlative study of magnetic flux transfer in the magnetosphere. *J. geophys. Res.* **83**, 3831.

Holzer, R. E. and Slavin, J. A. (1982) An evaluation of three predictors of geomagnetic activity. *J. geophys. Res.* **87**, 2558.

Holzer, R. E. and Slavin, J. A. (1983) Reply. *J. geophys. Res.* **88**, 4955.

Jorgensen, T. S., Friis-Christensen, E., Wickwar, V. B., Kelly, J. D., Clauer, C. R. and Banks, P. M. (1984) On the reversal from "sunward" to "antisunward" plasma convection in the dayside high latitude ionosphere. *Geophys. Res. Lett.* **11**, 887.

Killeen, T. L., Heelis, R. A., Hays, P. B., Spencer, N. W. and Hanson, W. B. (1985) Neutral motions in the polar thermosphere for northward interplanetary magnetic field. *Geophys. Res. Lett.* **12**, 159.

Lockwood, M., van Eyken, A. P., Bromage, B. J. I., Waite, J. H., Jr., Moore, T. E. and Doupnik, J. R. (1986a) Low-energy ion outflows from the ionosphere during a major polar cap expansion—evidence for equatorward motion of inverted-V structures. *Adv. Space Res.* **6**, 93.

Lockwood, M., van Eyken, A. P., Bromage, B. J. I., Willis, D. M. and Cowley, S. W. H. (1986b) Eastward propagation of a plasma convection enhancement following a southward turning of the interplanetary magnetic field. *Geophys. Res. Lett.* **13**, 72.

Lühr, H., Klocker, N., Oelschlagel, W., Hausler, B. and Acuna, M. (1985) The *IRM* fluxgate magnetometer. *IEEE Trans. Geosci. Remote Sensing* **GE-23**, 259.

McPherron, R. L. and Manka, R. H. (1985) Dynamics of the 10:54 U.T. March 2, 1979 substorm event: CDAW 6. *J. geophys. Res.* **90**, 1175.

Meloni, A., Wolfe, A. and Lanzerotti, L. J. (1982) On the relationship between interplanetary quantities and the global auroral electrojet index. *J. geophys. Res.* **87**, 119.

Murayama, T. (1982) Coupling function between solar wind parameters and geomagnetic indices. *Rev. Geophys. Space Phys.* **20**, 623.

Nishida, A. (1968a) Geomagnetic DP 2 fluctuations and associated magnetospheric phenomena. *J. geophys. Res.* **73**, 1795.

Nishida, A. (1968b) Coherence of geomagnetic DP 2 fluctuations with interplanetary magnetic variations. *J. geophys. Res.* **73**, 5549.

Nishida, A. and Kamide, Y. (1983) Magnetospheric processes preceding the onset of an isolated substorm: a case study of the March 31, 1978 substorm. *J. geophys. Res.* **88**, 7005.

Oliver, W. L., Holt, J. M., Wand, R. H. and Evans, J.V. (1983) Millstone Hill incoherent scatter observations of auroral zone convection over $60° < \lambda < 75°$: average patterns vs K_p. *J. geophys. Res.* **88**, 5505.

Paschmann, G., Papamastorakis, I., Baumjohann, W., Sckopke, N., Carlson, C. W., Sonnerup, B. U. O. and Luhr, H. (1986) The magnetopause for large magnetic shear: *AMPTE/IRM* observations. *J. geophys. Res.* **91**, 11099.

Pellinen, R. J., Baumjohann, W., Heikkila, W. J., Sergeev, V. A., Yahnin, A. G., Marklund, G. and Melnikov, A. O. (1982) Event study on pre-substorm phases and their relation to the energy coupling between the solar wind and magnetosphere. *Planet. Space Sci.* **30**, 371.

Perreault, P. and Akasofu, S.-I. (1978) A study of geomagnetic storms. *Geophys. J. R. astr. Soc.* **54**, 547.

Quegan, S., Bailey, G. J., Moffett, R. J., Heelis, R. A., Fuller-Rowell, T. J., Rees, D. and Spiro, R. W. (1982) A theoretical study of the distribution of ionization in the high-latitude ionosphere and the plasmasphere: first results on the mid-latitude trough and the light-ion trough. *J. atmos. terr. Phys.* **44**, 619.

Rees, D., Fuller-Rowell, T. J., Gordon, R., Smith, M. F., Maynard, N. C., Spencer, N. W., Wharton, L., Hays, P. B. and Killeen, T. L. (1986) A theoretical and empirical study of the response of the high latitude thermosphere to the sense of the "*Y*" component of the interplanetary magnetic field. *Planet. Space Sci.* **34**, 1.

Reiff, P. H., Spiro, R. W. and Hill, T. W. (1981) Dependence of polar cap potential drop on interplanetary parameters. *J. geophys. Res.* **86**, 7639.

Rijnbeek, R. P., Cowley, S. W. H., Southwood, D. J. and Russell, C. T. (1984) A survey of dayside flux transfer events observed by *ISEE* 1 and 2 magnetometers. *J. geophys. Res.* **89**, 786.

Rishbeth, H., Smith, P. R., Cowley, S. W. H., Willis, D. M., van Eyken, A. P., Bromage, B. J. I. and Crothers, S. R. (1985) Ionospheric response to changes in the interplanetary magnetic field observed by EISCAT and *AMPTE UKS*. *Nature* **318**, 451.

Schatten, K. H. and Wilcox, J. M. (1967) Response to geomagnetic activity index K_p to the interplanetary magnetic field. *J. geophys. Res.* **72**, 5185.

Southwood, D. J., Mier-Jedrzejowicz, W. A. C. and Russell, C. T. (1985) The fluxgate magnetometer for the *AMPTE UKS* subsatellite. *IEEE Trans. Geosci. Remote Sensing* **GE-23**, 301.

Spreiter, J. R. and Stahara, S. S. (1980) A new predictive model for determining solar wind–terrestrial planet interactions. *J. geophys. Res.* **85**, 6769.

Todd, H., Bromage, B. J. I., Cowley, S. W. H., Lockwood, M., van Eyken, A. P. and Willis, D. M. (1986) EISCAT observations of bursts of rapid flow in the high latitude dayside ionosphere. *Geophys. Res. Lett.* **13**, 909.

Todd, H., Cowley, S. W. H., Etemadi, A., Bromage, B. J. I., Lockwood, M., Willis, D. M. and Lühr, H. (1988) Flow in the high latitude ionosphere: measurements at 15 seconds resolution made using the EISCAT "Polar" experiment. *J. atmos. terr. Phys.*, in press.

Tsurutani, B. T. and Meng, C.-I. (1972) Interplanetary magnetic field variations and substorm activity. *J. geophys. Res.* **77**, 2964.

Tsurutani, B. T., Slavin, J. A., Kamide, Y., Zwickl, R. D., King, J. H. and Russell, C. T. (1985) Coupling between

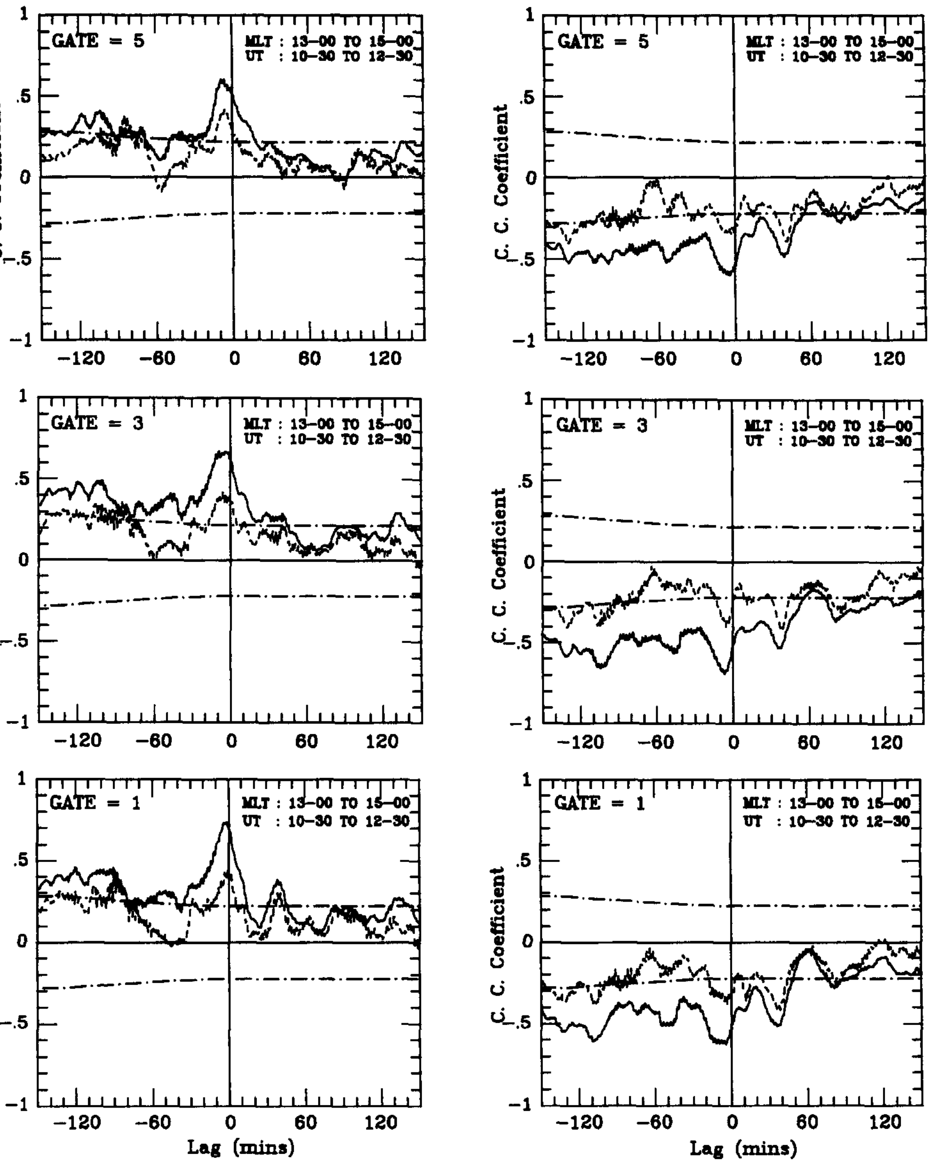

FIG. A1. CORRELOGRAMS OF THE IONOSPHERIC FLOW COMPONENTS AND TWO FUNCTIONS OF SOLAR WIND/IMF PARAMETERS ARE SHOWN FOR GATES 1, 3 AND 5, IN THE 2 h M.L.T. SECTOR CENTRED ON 14:00 M.L.T. (WHERE THESE CORRELATIONS ARE STRONGEST).

Solid lines show results using V^2B_S, and dashed lines ε. Results for V_E are shown on the left side of the figure, while results for V_N are shown on the right. As in Fig. 4, the dot-dash line indicates the 99.9% significance level.

the solar wind and the magnetosphere: CDAW6. *J. geophys. Res.* **90**, 1191.

Wickwar, V. B., Kelly, J. D., de la Beaujardiere, O., Leger, C. A., Steenstrup, F. and Dawson, C. H. (1984) Sondrestrom overview. *Geophys. Res. Lett.* **11**, 883.

Willis, D. M., Lockwood, M., Cowley, S. W. H., van Eyken, A. P., Bromage, B. J. I., Rishbeth, H., Smith, P. R. and Crothers, S. R. (1986) A survey of simultaneous observations of the high-latitude ionosphere and interplanetary magnetic field with EISCAT and *AMPTE–UKS*. *J. atmos. terr. Phys.* **48**, 987.

Wygant, J. R., Torbert, R. B. and Mozer, F. S. (1983) Comparison of S3-3 polar cap potential drops with the interplanetary magnetic field and models of magnetopause reconnection. *J. geophys. Res.* **88**, 5727.

APPENDIX

In this appendix we briefly report the results of a preparatory study which was undertaken to determine the function of solar wind and IMF parameters which should best be used in the cross-correlation analysis reported in this paper. To this end, correlograms were derived (as in Section 3) using a variety of such functions, with the aim of finding the function which gave the highest and clearest peaks. The functions investigated included B_z, VB_z, V^2B_z, B_S, VB_S, V^2B_S and ε (as defined in Section 1).

Particular attention was paid to the early afternoon sector where correlation effects tend to be clearest. It was found that, generally, V^2B_S gives the highest peak values, as illustrated in Fig. A1. Correlograms are shown for the 2 h interval centred on 14:00 M.L.T. in a similar format to those shown on the left side of Fig. 4. Here, however, solid lines refer to V^2B_S and dashed lines to ε. Results for V_E are shown on the left side of the figure, while those for V_N are shown on the right. It can be seen that in general V^2B_S provides a peak near zero lag which has a larger value of the cross-correlation coefficient and is better defined than for ε. The correlograms for the other parameters investigated generally lie between these two limits. Consequently V^2B_S was chosen as the parameter to be employed in the cross-correlation analysis presented in this paper.